

SANDIA REPORT

SAND2005-7144

Unlimited Release

Printed December 2005

Uncertainty Analysis of Steady State Incident Heat Flux Measurements in Hydrocarbon Fuel Fires

James T. Nakos

Prepared by
Sandia National Laboratories
Albuquerque, New Mexico 87185 and Livermore, California 94550

Sandia is a multiprogram laboratory operated by Sandia Corporation, a Lockheed Martin Company, for the United States Department of Energy's National Nuclear Security Administration under Contract DE-AC04-94AL85000.

Approved for public release; further dissemination unlimited.



Issued by Sandia National Laboratories, operated for the United States Department of Energy by Sandia Corporation.

NOTICE: This report was prepared as an account of work sponsored by an agency of the United States Government. Neither the United States Government, nor any agency thereof, nor any of their employees, nor any of their contractors, subcontractors, or their employees, make any warranty, express or implied, or assume any legal liability or responsibility for the accuracy, completeness, or usefulness of any information, apparatus, product, or process disclosed, or represent that its use would not infringe privately owned rights. Reference herein to any specific commercial product, process, or service by trade name, trademark, manufacturer, or otherwise, does not necessarily constitute or imply its endorsement, recommendation, or favoring by the United States Government, any agency thereof, or any of their contractors or subcontractors. The views and opinions expressed herein do not necessarily state or reflect those of the United States Government, any agency thereof, or any of their contractors.

Printed in the United States of America. This report has been reproduced directly from the best available copy.

Available to DOE and DOE contractors from

U.S. Department of Energy
Office of Scientific and Technical Information
P.O. Box 62
Oak Ridge, TN 37831

Telephone: (865) 576-8401
Facsimile: (865) 576-5728
E-Mail: reports@adonis.osti.gov
Online ordering: <http://www.osti.gov/bridge>

Available to the public from

U.S. Department of Commerce
National Technical Information Service
5285 Port Royal Rd.
Springfield, VA 22161

Telephone: (800) 553-6847
Facsimile: (703) 605-6900
E-Mail: orders@ntis.fedworld.gov
Online order: <http://www.ntis.gov/help/ordermethods.asp?loc=7-4-0#online>



Uncertainty Analysis of Steady State Incident Heat Flux Measurements in Hydrocarbon Fuel Fires

James T. Nakos
Fire Science and Technology Department
Sandia National Laboratories
PO Box 5800
Albuquerque, NM 87185

Abstract

The objective of this report is to develop uncertainty estimates for three heat flux measurement techniques used for the measurement of incident heat flux in a combined radiative and convective environment. This is related to the measurement of heat flux to objects placed inside hydrocarbon fuel (diesel, JP-8 jet fuel) fires, which is very difficult to make accurately (e.g., less than 10%). Three methods will be discussed: a Schmidt-Boelter heat flux gage; a calorimeter and inverse heat conduction method; and a thin plate and energy balance method. Steady state uncertainties were estimated for two types of fires (i.e., calm wind and high winds) at three times (early in the fire, late in the fire, and at an intermediate time). Results showed a large uncertainty for all three methods. Typical uncertainties for a Schmidt-Boelter gage ranged from $\pm 23\%$ for high wind fires to $\pm 39\%$ for low wind fires. For the calorimeter/inverse method the uncertainties were $\pm 25\%$ to $\pm 40\%$. The thin plate/energy balance method the uncertainties ranged from $\pm 21\%$ to $\pm 42\%$. The 23-39% uncertainties for the Schmidt-Boelter gage are much larger than the quoted uncertainty for a radiative only environment (i.e., $\pm 3\%$). This large difference is due to the convective contribution and because the gage sensitivities to radiative and convective environments are not equal. All these values are larger than desired, which suggests the need for improvements in heat flux measurements in fires.

Acknowledgements

The author would like to acknowledge the support of several colleagues. Financial support was provided by the W76-1 Qualification Program (Tom Hendrickson, Qualification Team Lead), and by Campaign 6, the Weapon System Engineering Certification Program (Lou Gritzo, Abnormal Thermal Environments program manager). Prof. Tom Diller from Virginia Tech University provided the Schmidt-Boelter calibrations in convective environments. Prof. Diller, Dr. Tom Blanchat, and Dr. Ben Blackwell reviewed this document and provided feedback. Dr. Walt Gill and Dr. Alex Brown provided valuable technical support and guidance for determining some of the parameters. All of this assistance was greatly appreciated.

Table of Contents

1	Executive Summary.....	7
2	Introduction.....	8
3	Background	10
4	Methodology.....	12
5	Global Definition of Fire Environment.....	15
5.1	Temperatures	15
5.2	Surface Properties	15
5.3	Radiation Heat Transfer from Fire	15
5.4	Convection.....	16
6	Determination of the Heat Flux Uncertainty.....	21
6.1	Schmidt-Boelter Type Heat Flux Gage – Net Flux Uncertainty	21
6.2	Calorimeter and Inverse Heat Conduction Method – Net Flux Uncertainty.....	25
6.3	Energy Balance Method – Incident Heat Flux Uncertainty.....	26
6.3.1	Thin Plate Gage Background	26
6.3.2	Thin Plate Gage Applied to Calm and Windy Fires	29
7	Examples.....	31
7.1	S-B Type Gage.....	31
7.1.1	Low Wind Case	31
7.1.2	High Wind Case	33
7.2	Calorimeter and Inverse Heat Conduction Method	34
7.2.1	Low Wind Case	34
7.2.2	High Wind Case	38
7.2.3	Late Times.....	40
7.3	Energy Balance Method/Thin Plate Gage.....	41
7.3.1	Low Wind Fire	41
7.3.2	High Wind Fire.....	47
8	Discussion	52
9	Conclusions.....	54
10	References	56

List of Figures

Figure 1	Energy Balance at Sensing Surface.....	13
Figure 2	Calorimeter Details.....	28
Figure 3:	Estimate of Surface Temperature Temporal Gradient for Thin Plate Gage, Low Wind Fire	43

List of Tables

Table 1: Reynolds Number Evaluations for Low Wind Fire	18
Table 2: Grashoff Number Evaluations, Low Wind Fire.....	18
Table 3: Gr_D/Re_D^2 Ratio Evaluations, Low Wind Fire	18
Table 4: Convective Heat Transfer Coefficient Evaluations for 30 cm Diameter Horizontal Cylinder, Calm Wind, 1300 K Gas Temperature	19
Table 5: Convective Heat Transfer Coefficient Evaluations for 30 cm Diameter Horizontal Cylinder, 10 m/s Wind, 1700 K Gas Temperature.....	21
Table 6: Parameters and Parameter Uncertainties for Use in Low Wind Case (100 kW/m ² net flux)	24
Table 7: Parameters and Parameter Uncertainties for Use in High Wind Case	25
Table 8: Parameter Values for the S-B Gage, Early Times, Low Wind Fire	32
Table 9: Relative Magnitude of Uncertainty Sources,	33
Table 10: Parameter Values for Early Times, S-B Gage, High Wind Case	34
Table 11: Relative Magnitude of Uncertainty Sources,	34
Table 12: Relative Magnitude of Uncertainty Sources,	35
Table 13: Parameter Values for Intermediate Times, Calorimeter, Low Wind Case	36
Table 14 Relative Magnitude of Uncertainty Sources,	36
Table 15 Parameter Values for Late Times, Calorimeter, Low Wind Case	37
Table 16: Relative Magnitude of Uncertainty Sources,	37
Table 17: Parameter Values for the Calorimeter, High Wind Case, Early Times	38
Table 18: Relative Magnitude of Uncertainty Sources,	38
Table 19: Parameter Values for the Calorimeter, Intermediate Times, High Winds	39
Table 20: Relative Magnitude of Uncertainty Sources,	39
Table 21: Parameter Values for Late Times, Calorimeter, High Wind Case.....	40
Table 22: Relative Magnitude of Uncertainty Sources,	40
Table 23: Energy Balance Method/Thin Plate Gage Uncertainty –	42
Table 24: Relative Importance of Uncertainty Terms,	43
Table 25: Energy Balance Method/Thin Plate Gage Uncertainty –	44
Table 26: Relative Importance of Uncertainty Terms,	45
Table 27 Energy Balance Method/Thin Plate Gage Uncertainty –	45
Table 28 Relative Importance of Uncertainty Terms,	46
Table 29 Energy Balance Method/Thin Plate Gage Uncertainty –	47
Table 30 Relative Importance of Uncertainty Terms,	48
Table 31 Energy Balance Method/Thin Plate Gage Uncertainty –	49
Table 32 Relative Importance of Uncertainty Terms,	50
Table 33 Energy Balance Method/Thin Plate Gage Uncertainty –	50
Table 34: Relative Importance of Uncertainty Terms,	51
Table 35 Summary of Uncertainty Estimates for Incident Radiative Flux.....	52
Table 36 Parameters Having Largest Effect on Total Uncertainty.....	52

1 Executive Summary

The objective of this report is to develop uncertainty estimates for three heat flux measurement techniques used for the measurement of incident heat flux in a combined radiative and convective environment. This has application to the measurement of heat flux to objects placed inside hydrocarbon fuel (diesel, JP-8 jet fuel) fires, which is a very difficult measurement to make accurately (e.g., less than 10%). It would be desirable to obtain incident heat flux levels consistently less than $\pm 10\%$ in all cases, but because of the difficulty of making these measurements, and the severe environment, a more realistic value would be $\pm 15\text{-}20\%$. The incident heat flux to objects in a hydrocarbon fuel fire is important because with it one can assess the threat posed by the fire, but the net absorbed flux is important for gage survivability. Three methods were evaluated: 1) a commercially available Schmidt-Boelter (S-B) heat flux gage; 2) a calorimeter/inverse heat conduction method; and 3) a thin plate gage/energy balance method.

Results showed relatively large steady state uncertainties for all three methods: 1) $\pm 39\%$ for low wind fires to $\pm 23\%$ for high wind fires for the S-B gage; 2) $\pm 40\%$ for low wind fires to $\pm 25\%$ for high wind fires for the calorimeter/inverse method; and 3) $\pm 42\%$ at low winds to $\pm 21\%$ at high winds for the thin plate/energy balance method. These results are shown in Tabular form in Table 35 in Section 8.

The uncertainties are greater for transient measurements than the steady state values listed above because the transient response of the thin plate method and calorimeter/inverse heat conduction method is poor. Because typical hydrocarbon fuel fires are highly fluctuating, and therefore mostly transient, it is likely that our measures of transient heat fluxes in fires are less accurate than the values for steady measurements.

2 Introduction

The measurement of heat flux in hydrocarbon fuel fires is difficult due to the high temperatures (e.g., 1000°C or higher), and the sooty and chemically reactive environment. Many commercially available sensors do not work well in fires because they are water-cooled. Soot builds up on the sensing surface due to thermophoresis and this layer of soot changes the gage sensitivity. Post-test soot deposit thicknesses of 1/4" have been seen in large fires at Sandia National Laboratories (SNL). Eliminating use of water-cooled gages, or just partially cooling the gages, or using gas purging, would reduce or eliminate the soot deposition, however, many non-cooled gages do not survive in long duration fire environments, or the gage sensitivity is not constant with the sensor temperature. Therefore, many commercially available gages do not work well when trying to measure heat flux inside a sooty fire, but do work adequately outside the fire, away from the soot.

Other sensor types are not actively cooled. An example is a relatively simple device called a "calorimeter." Calorimeters are made of metals that do survive fires (e.g., 304 stainless steel (SS)) with a thermocouple (TC) on the cold side backed with insulation. Net flux into the hot surface can be estimated using temperature measurements of the cold surface and assumptions about the cold side boundary condition. Inverse heat conduction codes (e.g., IHCP1D (ref. [1]) or SODDIT (ref. [2])) can estimate the exposed surface net flux. One-dimensional heat conduction is almost always assumed to simplify the calculations. If the heat transfer is not 1-dimensional, an added element of uncertainty is present.

In commercially available heat flux gages (e.g., Gardon or Schmidt-Boelter) and inverse heat conduction methods a voltage is generated based on the net amount of energy into the sensing surface. Based on the calibration method, this net energy can be related to either an incident radiative flux or a net flux. In fire applications, an estimate of the heat flux (both radiative and convective) incident on the gage surface is desired. Net flux cannot be used for other surfaces because every surface will absorb energy differently. This is not to suggest that the incident flux (especially the convective heat transfer coefficient) is totally independent of surface properties. Also, for thermally massive test objects, the fire is affected. However for this discussion, the incident flux is assumed to not be affected by surface properties because normally heat flux gages are small relative to the fire.

Due to the severe environment and difficulty of measuring the required parameters, the measurement of net heat flux in hydrocarbon fuel fires usually has large uncertainties (e.g., $\pm 20\%$ using an inverse heat conduction code (ref. [3])). Two-dimensional effects can add additional uncertainty, e.g., 2-20% depending on the degree of 2-dimensionality (ref. [4]). Uncertainties of similar magnitude can occur when one estimates incident flux given net flux from an S-B or Gardon type gage because of soot deposition on the sensor face, and from convective effects.

A third type of measurement will be called the "energy balance method." In this case the temperature of a thin flat surface is measured and an energy balance is developed on that surface. Heat flux from a hemisphere surrounding the flat plate is part of the energy balance. From the energy balance one can estimate the incident heat flux. This method has been used successfully to estimate steady incident heat flux in fires (refs. [4], and [5]).

This report develops uncertainty quantification analyses (UQA) and uncertainty estimates for the conversion of net to incident flux when using three methods: 1) an S-B heat flux gage; 2) a calorimeter/inverse heat conduction method; and a thin plate gage/energy balance method. The methods were evaluated in two “typical” hydrocarbon fuel fires for three times of interest (early when the object temperature is close to the initial value, late, when the object’s surface temperature has equilibrated to the fire temperature, and an intermediate time). The two fires are those in calm winds when total maximum flux levels are about 100 kW/m², and in high winds (e.g., 10 m/s) when the flux levels are about 380 kW/m². (These fluxes are arbitrarily chosen but are representative.)

3 Background

A number of different types of commercially available heat flux gages are available. Gardon (circular foil) gages, Schmidt-Boelter (S-B) gages, thermopile type gages, and “thin film” gages are a few. Childs, et al. (ref. [6]) provide a comprehensive listing of heat flux measurement techniques. Optical devices are also used to infer heat flux if the emissivity of the radiating surface is known. Optical sensors are normally grouped into two types, thermal and photon detectors (ref. [7]). All types of gages respond to the energy net by the sensing surface, except photon detectors which respond to the incident radiative flux. This analysis focuses only on non-optical detectors.

The sensitivity of a typical non-optical type gage (e.g., Schmidt-Boelter, Gardon, thin film, etc.) is usually determined by a radiative calibration in a blackbody type furnace. These calibration devices are typically designed so that convection is negligible. If this is so, then the conversion from net to incident is straightforward (assuming the absorptivity is constant with wavelength or the application has the same radiative spectrum as the calibration source, and if the gage temperature is low enough); one divides the net flux by the surface absorptivity to obtain the incident flux. Alternatively, one can compare the output of the gage to a known calibration source to directly obtain the incident radiative flux.

In combined environments (radiative and convective), one cannot make this conversion unless the gage sensitivity to convective heat flux is the same as for radiative heat flux. Recent measurements on a Schmidt-Boelter gage showed that the convective sensitivity (i.e., kW/m²/mV) coefficient was about 12% lower for convection (ref. [8]). Therefore, to obtain an accurate estimate of the incident flux to a surface with both radiative and convective heat transfer present, one needs to know both the radiative and convective gage sensitivities, and the fractions of the total net flux from radiation and convection. The convective and radiative fractions are not accurately known in fire environments, and can vary with time. Manufacturers normally only calibrate their gages in radiative environments, so convective calibration factors are not known.

An alternate method of estimating the effect of convection on the gage calibration was developed by Kuo and Kulkarni (ref. [9]) who studied the sensitivity of Gardon type gages to a mixed environment consisting of both radiative and convective parts. They showed that for Gardon gages (calibrated in radiative-only environments), significant errors could occur under certain conditions of large gage sensing surface and large convective heat transfer coefficients. For a free convection vertical wall fire experiment, an error of about 15% would occur by using the sensitivity provided by the manufacturer. In other words, the gage sensitivity to convective heating was different than for radiative heating. Kuo and Kulkarni developed correction factors for different sized gages and convective heat transfer coefficients.

Borell and Diller (ref. [10]) evaluated a convective calibration method for Gardon type gages. They found that the convective calibration was non-linear, whereas a radiation calibration is linear to within a few percent (e.g., $\pm 3\%$). Borell and Diller noted that radiative calibration methods deliver a constant *heat flux* to the gage surface, whereas a convective calibration method delivers a constant *convective heat transfer coefficient* to the gage surface. This causes different results for the two types of calibrations, due to different temperature profiles on the gage surface. Strictly speaking, these results only apply to the Gardon type gage which under radiative flux conditions

has a parabolic-type temperature profile on the sensing surface. Schmidt-Boelter (S-B) type gages have a much flatter temperature profile on the gage surface. However, as indicated above, recent evidence shows that S-B type gages also have different gage sensitivities to radiative and convective heat transfer [8].

Robertson and Ohlemiller (ref. [11]) discuss heat flux measurements in low radiation environments. The desired measurement was the incident radiative flux to a surface. In these low radiation environments one has to be sure to account for the gage surface temperature, a function of the cooling water temperature. An apparent output occurs if the gage surface temperature is either above or below the effective radiation temperature of the surroundings. In addition, convective input to the gage when mounted in a vertical structure was apparent when testing the gage with and without the mounting structure in place. These two effects show the importance of understanding gage calibration and operation in the particular application of interest.

Bryant, et al. (ref. [12]) studied the uncertainty of incident radiative heat flux measurements estimated from total heat flux measurements for gages placed outside but near a typical room corner fire specified by ISO 9705 (ref. [13]). In this case, a Schmidt-Boelter (S-B) gage was located some distance away from the fire. The gage was water-cooled without (presumably) having the gage surface fouled by soot deposition. The uncertainty methodology used in Bryant, et al. (ref. [12]) consisted of establishing a control volume around the sensing surface, then developing an energy balance. In this manner the incident radiative flux was related to the net flux, the convective flux and a re-radiation term. An uncertainty analysis was performed on each of these parameters by using sensitivity coefficients. Uncertainties in each of the parameters were determined from measurements, general knowledge, or manufacturer's specifications. A root-sum-square method was used to combine the individual uncertainties. Results showed that for the case considered one could estimate radiative flux from total flux measurements to within about 20%, but only with a confidence level of about 67% or 1σ . The uncertainty methodology by Bryant et al. will be used in this report.

4 Methodology

It will be apparent later that parameter uncertainty estimates are themselves uncertain, so precisely subscribing a confidence level (e.g., 2σ or 95%) cannot be confidently justified. However, large uncertainties were used wherever possible, so a 95% confidence level will be assumed.

Figure 1 shows a schematic of the surface being analyzed. This is the sensing surface of the gage, subjected to a mixed environment consisting of both radiative and convective fluxes, an environment typical of a hydrocarbon fuel fire. The radiative heat flux dominates. A control volume is drawn over the sensing surface. The net heat flux net into the surface (q_{net}) is a function of the incident radiative flux ($q_{inc,r}$), the surface properties (emissivity ε and absorptivity α), the emitted flux ($q_{emit} = \varepsilon\sigma T_s^4$), and the convective heat gain or loss, $q_{conv} = h(T_\infty - T_s)$. It is further assumed that there is neither condensation nor any chemical reactions that could change the heat flux to the surface. T_s is the surface temperature, h is the convective heat transfer coefficient, and T_∞ is the free stream gas temperature.

Equation {1} expresses the overall energy balance on the control volume surrounding the gage surface:

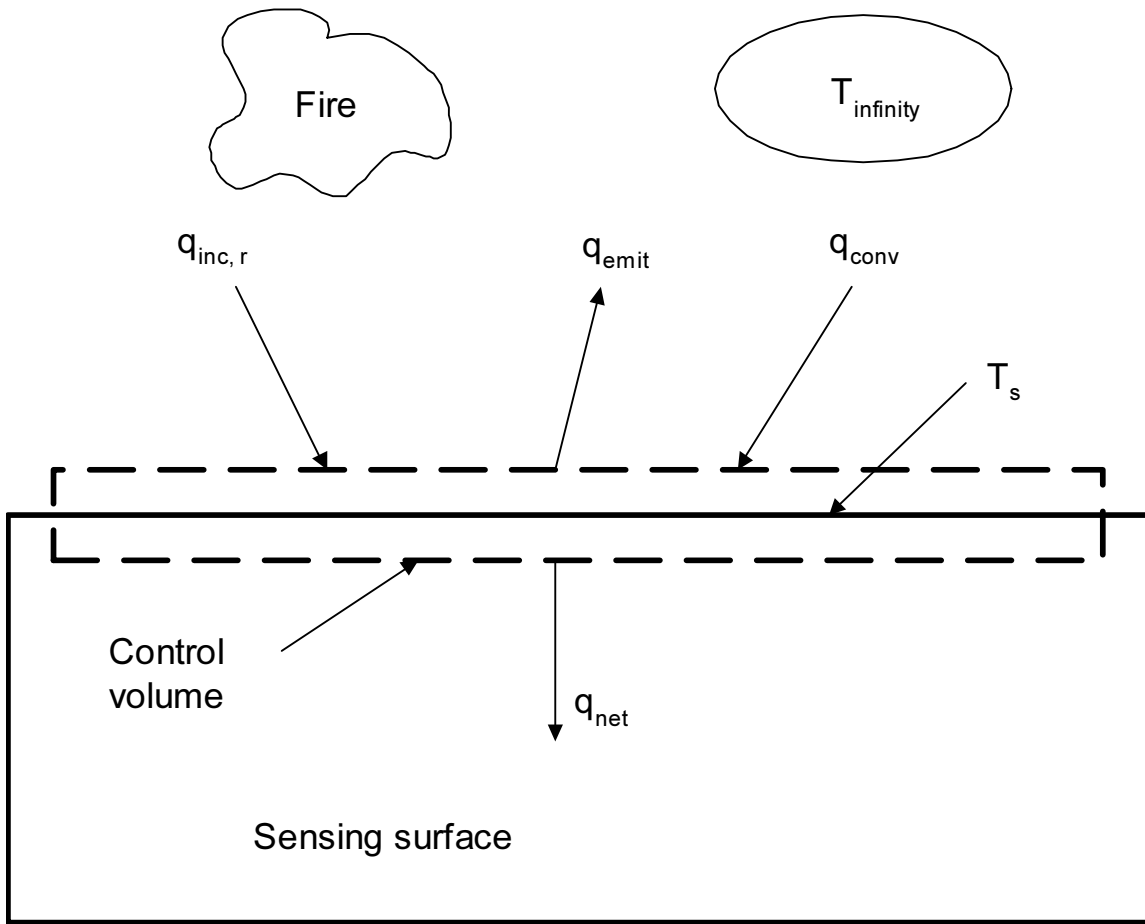
$$q_{net} = \alpha q_{inc,r} - q_{emit} + q_{conv}. \quad \{1\}$$

The “net” flux is the sum of the first and last terms in equation {1}. The “net” flux is the net flux minus the emitted flux. Substituting for q_{emit} and q_{conv} :

$$q_{net} = \alpha q_{inc,r} - \varepsilon\sigma T_s^4 + h(T_\infty - T_s). \quad \{2\}$$

Normally, one invokes the assumption that $\alpha = \varepsilon$ for a gray body and that will be done here. Rearranging equation {2} one can solve for $q_{inc,r}$, the incident radiative flux:

$$q_{inc,r} = (q_{net} / \varepsilon) + \sigma T_s^4 - (h / \varepsilon)(T_\infty - T_s). \quad \{3\}$$



- $q_{inc,r}$ = incident radiative flux
- q_{emit} = emitted flux
- q_{conv} = convective flux
- q_{net} = absorbed flux

Figure 1 Energy Balance at Sensing Surface

Alternatively, the total flux incident on the surface is the sum of the incident radiative part and the convective part:

$$q_{inc,t} = q_{inc,r} + h(T_{\infty} - T_s). \quad \{4\}$$

The net flux can be obtained from several methods. For example one can use a Schmidt-Boelter gage or one can obtain the net flux from a calorimeter/inverse heat conduction method. These cases will be analyzed separately.

Equation {3} can be used to determine incident radiative flux given the parameters in the equation. The total flux incident on the surface is then the incident radiative part ($q_{inc,r}$) plus the convective flux (q_{conv}).

The conversion to incident radiative flux is difficult because the parameters in equation {3} are difficult to accurately determine and therefore have large uncertainties. For example, the convective heat transfer coefficient (h) may have both free and forced convective components. The fire generates a buoyant flow upward (free convection), and wind creates a cross flow (forced convection). This environment is not addressed in typical convective heat transfer correlations. Even in tightly controlled experiments, $\pm 25\%$ uncertainties in heat transfer coefficients are not uncommon (ref. [14]). Also, the accurate determination of the net flux, free stream temperature T_∞ and the surface temperature T_s is difficult because they vary with time and space.

To obtain an estimate of the uncertainty in incident radiative flux, the method used by Bryant, et al., and described in refs. [14], [15], or [16] was used. The partial derivative of each term in equation {3} is evaluated and the results using a root-sum-square method are combined. Equation {5} expresses the total uncertainty in the incident radiative flux:

$$\Delta q_{inc,r} = [((\partial q_{inc,r} / \partial q_{net}) \Delta q_{net})^2 + ((\partial q_{inc,r} / \partial \varepsilon) \Delta \varepsilon)^2 + \dots]^{1/2}. \quad \{5\}$$

The partial derivatives are called sensitivity coefficients. Evaluating the sensitivity coefficients one obtains the following:

$$\begin{aligned} \partial q_{inc,r} / \partial q_{net} &= 1 / \varepsilon \\ \partial q_{inc,r} / \partial \varepsilon &= -q_{net} / \varepsilon^2 + (h / \varepsilon^2)(T_\infty - T_s) \\ \partial q_{inc,r} / \partial T_s &= 4\sigma T_s^3 + h / \varepsilon \\ \partial q_{inc,r} / \partial h &= (-1 / \varepsilon)(T_\infty - T_s) \\ \partial q_{inc,r} / \partial T_\infty &= -h / \varepsilon \end{aligned} \quad \{6\}$$

Therefore, the total uncertainty in incident radiative flux ($\Delta q_{inc,r}$) is:

$$\Delta q_{inc,r} = [(\Delta q_{net} / \varepsilon)^2 + (((-q_{net} / \varepsilon^2) + (h / \varepsilon^2)(T_\infty - T_s)) \Delta \varepsilon)^2 + ((4\sigma T_s^3 + h / \varepsilon) \Delta T_s)^2 + ((-1 / \varepsilon)(T_\infty - T_s) \Delta h)^2 + ((-h / \varepsilon) \Delta T_\infty)^2]^{1/2} \quad \{7\}$$

If all the individual uncertainty estimates (Δq_{net} , $\Delta \varepsilon$, etc.) are known with a certain level of confidence (e.g., 95%), then the result in equation {7} will also have the same level of confidence. Key in evaluating the incident radiative flux uncertainty is the evaluation of the uncertainty in the net flux, q_{net} . Evaluation of this parameter for both an S-B type gage and the calorimeter/inverse heat conduction method will be performed after other parameters are defined.

5 Global Definition of Fire Environment

It is assumed that the gage is fully engulfed in an optically thick, sooty, hydrocarbon fuel fire. This normally means that the fire thickness is at least 1 meter and completely surrounds the object.

5.1 Temperatures

Typical “fire” or “flame” temperatures (effective temperature of total incoming flux) measured using 1.6 mm diameter inconel sheathed, Type K (chromel-alumel), ungrounded junction TCs in JP-8 fires are about 1000°C or 1300 K (ref. [17]). These are typical of low wind fires. The temperature of an un-cooled surface will eventually equilibrate with the fire. Therefore, the final surface temperature T_s will be assumed to be about 1300 K. The initial surface temperature is assumed to be 300 K.

T_∞ is the free stream temperature (“gas” temperature) and can be higher or lower than the value measured by the TC, depending on where one is in a fire. A typical gas temperature is about 1300 K in hydrocarbon fuel fires (ref. [18]) for low wind fires, and up to 1700°C¹ for high wind fires.

5.2 Surface Properties

The surface properties of the object are absorptivity and emissivity. It is assumed that the surface is diffuse gray and that the absorptivity and emissivity are equal. This is believed to be a good assumption because the surface is normally painted black, or heavily oxidized. In either case a high value of emissivity will be assumed, namely 0.85, consistent with measurements made on Pyromark™ black paint (ref. [19]). An uncertainty of about ±10% (0.09 emissivity units) will be assumed, also from the same reference.

5.3 Radiation Heat Transfer from Fire

The net flux is highest early in the fire but drops to zero as the surface temperature approaches the fire temperature. Early in the fire, the emitted flux is negligible, therefore the net flux can be expressed as follows:

$$q_{net} = \alpha q_{inc,r} + h(T_\infty - T_s) \quad \{8\}$$

where:

$$q_{inc,r} = \varepsilon_f F \sigma T_f^4 \quad \{9\}$$

In equation {9}, ε_f is the “fire” emissivity, F is the view factor between the fire and the object, and T_f is the fire or flame temperature. In this case F is assumed to be 1.0. The flame emissivity is often assumed to be high (e.g., 0.9) (ref. [20]). However, recent measurements by Kearney, 2001 (ref.

¹ The 1700°C value was estimated based on heat flux measurements of 400 kW/m² in high wind fires.

[21]) have shown the emissivity is lower (e.g., 0.4) but the temperature is higher for small fires in calm winds. Kearney's measurements showed an emissivity of 0.4, and a fire temperature of 1419 K fit the data well for a 1 m diameter JP-8 pool fire in low winds. Using these two values (emissivity = 0.4 and 1419 K temperature) and a view factor of 1.0, the estimated radiative incident flux is about 92 kW/m², in the middle of the range of fluxes seen in low wind fires. Assuming a surface emissivity of 0.85, the first term in equation {8} is about 79 kW/m². This will be used later.

Heat fluxes up to 400-450 kW/m² have been measured in fires driven by high winds (e.g., 10 m/s) (ref. [22]). In these cases the incident radiative flux from the fire is much higher than for the calm wind case. To obtain these high fluxes, the effective flame temperature has to be much higher than 1300 K. The adiabatic flame temperature of JP-8 is about 2300 K, so this is an upper limit for the gas temperature. Stainless steel (Type 304) and inconel melt at about 1700 K, and we have melted TCs in high wind fires. Because un-cooled calorimeters (described below) use these materials, 1700 K will be the maximum gas and surface temperature used. At 1700 K and $\epsilon = 0.85$, the estimated flux is about 400 kW/m². A higher effective emissivity (0.85) was used only to obtain a flux near the upper limit of those observed experimentally – this assumption may not be justified but will be used to obtain the high fluxes needed. If the same emissivity as for low wind fires (0.4) is used, a gas temperature of 2050°C would be required, which approaches the approximate adiabatic flame temperature of 2300 K. Therefore, a flux of 400 kW/m² and a gas temperature of 1700 K will be used in high wind fires.

5.4 Convection

The convective input to the object is highest during the early stages of the fire, when the temperature difference is largest (assuming the convective heat transfer coefficient is constant). The fraction of the total flux from convection (K_{conv}) to an *uncooled* object in a large hydrocarbon fuel fire can be up to 10-20% of the total (ref. [23]). The convective contribution is likely highest at the early part of the fire when the temperature difference is largest (assumed to be 20%), dropping to lower values as the surface heats up and the temperature difference is reduced. The convective contribution late in the fire is assumed to be negligible because the surface temperature has equilibrated with the fire. In the middle portion of the fire the fraction is assumed to be about 10%. These estimates have large uncertainties.

Convective heat transfer in fires arises from two sources – free convection from buoyancy effects, and forced convection from wind (open fires) or ventilation (enclosed fires). Geometry and orientation are also important. To reduce the number of variables and use a representative test setup, the gage will be assumed to be mounted in a horizontal circular cylinder 30 cm (12") diameter. Even though the heat transfer coefficient varies around the cylinder surface, an average value will be used (ref. [24]).

The following ratio should be evaluated to determine what type of correlation should be used.

$$Gr_D / (Re_D)^2. \quad \{10\}$$

If this ratio is much greater than 1, then free convection dominates and forced convection is negligible (ref. [24]). Therefore, a free convection correlation should be used. If this ratio is much less than 1, forced convection dominates, free convection is negligible, and a forced convection correlation should be used.

The Grashoff number (Gr) is defined as follows:

$$Gr_D = g\beta(T_s - T_\infty)D^3 / \nu^2, \quad \{11\}$$

where g is the acceleration of gravity (9.8 m/s^2), β is the coefficient of thermal expansion ($1/T$ for ideal gases (T in absolute temperature)), T_s is the surface temperature, T_∞ is the free stream fluid temperature, ν is the kinematic viscosity, and D is the diameter of the cylinder (30 cm). Properties are evaluated at the "film temperature" $[(T_s + T_\infty)/2]$.

The Reynolds number Re_D is defined as follows:

$$Re_D = VD / \nu, \quad \{12\}$$

where V is the free stream gas velocity, and D and ν are the same as for the Grashoff number.

It is known that the gas in a fire is a complex combination of air, combustion products and soot. Properties of this mixture are difficult to determine so it will be assumed that the gas is only air, for which high temperature properties are readily available.

The gas (air) is assumed to be at 1300 K for the calm wind fire and 1700 K for the high wind fire. For a gas temperature of 1300 K and surface temperatures of 300, 800, and 1300 K the kinematic viscosity is shown in Table 1. Similarly, the coefficient of thermal expansion is $1/800$, $1/1050$, and $1/1300$.

Vertical gas velocity measurements in fires range from 5-10 m/s from 2.2-6.1 m above the base of the fire (ref. [25]). Three values will be used, namely 1, 5, and 10 m/s. The 1 m/s value is assumed to be slightly above the base of the fire. Using these values, the Reynolds numbers (Re_D) are as shown in Table 1.

Surface temperatures (T_s) early in the fire are close to the initial ambient temperature, assumed to be 300 K. At later times, when the object has equilibrated with the fire, the surface temperature is close to the gas temperature, 1300 K. At intermediate times the surface temperature will be between these extremes, assumed to be 800 K. The free stream gas temperature is assumed to be a constant 1300 K for the low wind fire. Table 2 shows Grashoff number evaluations for the different surface temperatures. Combining the results one can estimate the Gr_D/Re_D^2 ratio as shown in Table 3.

Table 1: Reynolds Number Evaluations for Low Wind Fire

Gas Velocity, m/s	Surface Temperature, T_s , K	Kinematic viscosity, ν , m ² /s	Reynolds Number, $Re_D=VD/\nu$
1	300	85×10^{-6}	3,530
5	300	85×10^{-6}	17,650
10	300	85×10^{-6}	35,300
1	800	132×10^{-6}	2,270
5	800	132×10^{-6}	11,350
10	800	132×10^{-6}	22,700
1	1300	185×10^{-6}	1,622
5	1300	185×10^{-6}	8,110
10	1300	185×10^{-6}	16,220

Table 2: Grashoff Number Evaluations, Low Wind Fire

Surface Temperature, T_s	Grashoff Number, Gr_D
300 K	4.5×10^7
800 K	7.2×10^6
1300 K	0

Table 3: Gr_D/Re_D^2 Ratio Evaluations, Low Wind Fire

Gas Velocity, m/s	Surface Temperature, T_s , K	Kinematic viscosity, ν , m ² /s	Reynolds Number, $Re_D=VD/\nu$	Grashoff Number, Gr_D	Gr_D/Re_D^2 ratio	Does forced or free convection dominate?*
1	300	85×10^{-6}	3,530	4.5×10^7	3.67	Free
5	300	85×10^{-6}	17,650	4.5×10^7	0.15	Forced
10	300	85×10^{-6}	35,300	4.5×10^7	0.04	Forced
1	800	132×10^{-6}	2,270	7.2×10^6	1.40	Free
5	800	132×10^{-6}	11,350	7.2×10^6	0.06	Forced
10	800	132×10^{-6}	22,700	7.2×10^6	0.01	Forced
1	1300	185×10^{-6}	1,622	0	0	Forced
5	1300	185×10^{-6}	8,110	0	0	Forced
10	1300	185×10^{-6}	16,220	0	0	Forced

** If Gr_D/Re_D^2 is > 1 , free convection dominates. If Gr_D/Re_D^2 is < 1 , forced convection dominates.

Results in Table 3 indicate that the convection is both free and forced, depending on the time/temperature regime. However, for all cases except the lowest velocity (1 m/s) and lowest surface temperature (300 K), forced convection is dominant. These values were calculated

assuming no wind. The addition of wind should drive all cases into the forced convective regime. Therefore, for simplicity, a forced convection correlation will be used.²

Incropera and DeWitt (ref. [24]) recommend use of a correlation developed by Churchill and Bernstein for forced convection over a horizontal cylinder, as follows:

$$\overline{Nu}_D = 0.3 + \left(\frac{0.62 Re_D^{1/2} Pr^{1/3}}{\left(1 + (0.4/Pr)^{2/3}\right)^{1/4}} \right) \left(1 + \left(Re_D / 282,000 \right)^{5/8} \right)^{4/5} \quad \{13\}$$

where Pr is the Prandtl number $(c_p \mu / k)^3$ and all properties are evaluated at the film temperature $\{(T_s + T_\infty) / 2\}$. \overline{Nu}_D is the average Nusselt number, defined as (hD/k) , where again k is evaluated at the film temperature. This correlation is applicable for all Reynolds numbers and Prandtl numbers in the range $Re_D Pr > 0.2$. For air, the Prandtl number is about 0.707 at 300 K and 0.719 at 1300 K, so the Reynolds * Prandtl product for the cases considered here is always > 0.2 , so the correlation (equation {13}) can be used. Because the Prandtl number does not vary appreciably, a constant value of 0.71 will be used. Table 4 shows Nusselt number evaluations for the range of Reynolds numbers in Table 1.

As can be seen in Table 4, the convective heat transfer coefficient (HTC) h ranges from about 5 to a maximum of about 21 W/m²-K. The HTC is more sensitive to the flow velocity than the surface temperature. For all three surface temperatures and 1 m/s velocity, the HTC is about 5-6 W/m²-K. For a 5 m/s velocity, h is about 13-14 W/m²-K, and for 10 m/s velocity the HTC is about 19-21 W/m²-K.

Table 4: Convective Heat Transfer Coefficient Evaluations for 30 cm Diameter Horizontal Cylinder, Calm Wind, 1300 K Gas Temperature

Gas Velocity, m/s	Surface Temperature, T _s , K	Reynolds Number, Re _D =VD/v	Nusselt Number, hD/k	Convective Heat Transfer Coefficient, h, W/m ² -K
1	300	3,530	30.6	5.9
5	300	17,650	73.8	14.1
10	300	35,300	111.0	21.2
1	800	2,270	24.4	5.6
5	800	11,350	57.6	13.3
10	800	22,700	85.4	19.7
1	1300	1,622	20.5	5.6
5	1300	8,110	47.8	13.1
10	1300	16,220	70.3	19.2

² It is perhaps counterintuitive that in the case of no wind the convection is in the forced regime. However, one can assume that buoyancy from combustion is the “force” that drives the flow into the forced regime.

³ c_p is the specific heat, μ is the viscosity, and k is the thermal conductivity.

⁴ h is the convective heat transfer coefficient (HTC), D is the characteristic dimension, in this case the diameter, and k is as before, the thermal conductivity.

One would expect that the vertical velocity is lowest near the base of the fire and highest at higher locations above the fire. Measurements by Schneider and Kent (ref. [25]), showed that the velocity does increase with height. Measurements were made from 2.2-6.1 m above the fire, and average velocities ranged from 5 m/s at the 2.2 m elevation to about 10 m/s at the 6.1 m elevation. There were no measurements at the base of the fire but the vertical velocity has to be zero at ground level. Therefore, unless the object is less than 2.2 m from the base of the fire, the velocity will be between 5-10 m/s. As a result, the relevant heat transfer coefficient values from Table 4 are between 15-21 W/m²-K. Because there is so much uncertainty in fluid properties, velocity and whether the correlation (equation {13}) is accurate for convection in fires, a large uncertainty of ±50% will be assumed.

Using the largest value from Table 4, 21 W/m²-K, the largest convective heat transfer contribution ($h(T_{\infty}-T_s)$) is about 21 kW/m². Using the incident radiative flux (Section 5.3) of 79 kW/m², the convective part is about 21% of the total. **Therefore, the maximum total net flux is assumed to be 100 kW/m² for the low wind case.**

For the high wind case a similar analysis was performed. Results are shown in Table 5. The 10 and 15 m/s velocities were based on a 10 m/s horizontal wind and a 1, 5, or 10 m/s vertical velocity. The vector speeds are about 10.0, 11.1, and 14.1 m/s. To simplify the calculations 10 and 15 m/s were used to span the range.

The convective heat transfer coefficients in Table 5 range from about 15 to 31 W/m²-K, so the maximum flux is about 43 kW/m². The incident radiative part was assumed to be 400 kW/m², so the total is about 383 kW/m² assuming a surface emissivity of 0.85, so the convective part is about 11% of the total. **The maximum total net flux is assumed to be 383 kW/m² for the high wind case.**

These values will be used below.

A similar analysis was performed by V. Nicolette⁵ to address convective effects in fires. Incident heat fluxes spanned between 23-475 kW/m², and flame temperatures from 800-1700 K. For free convection effects the estimated heat transfer coefficients ranged from 7.3-7.8 W/m²-K. Forced convection coefficients ranged from 13-22 W/m²-K for a steady 9 m/s velocity. Assuming mixed convection was most appropriate, Nicolette estimated the total convective heat transfer coefficients of 20-28 W/m²-K, depending on whether or not the forced flow aided the natural convection process or the forced convection was horizontal. These values compare well with those in Tables 4 and 5. The values from Tables 4 and 5 will be used here because all inputs are known.

⁵ Presentation by V. Nicolette, Sandia National Laboratories, October 5, 1998.

Table 5: Convective Heat Transfer Coefficient Evaluations for 30 cm Diameter Horizontal Cylinder, 10 m/s Wind, 1700 K Gas Temperature

Gas Velocity, m/s	Surface Temperature, T_s , K	Reynolds Number, $Re_D=VD/\nu$	Nusselt Number, hD/k	Convective Heat Transfer Coefficient, h , $W/m^2\cdot K$
10	300	24,590	89.5	24.5
15	300	36,890	114.0	31.2
10	1000	15,000	67.3	18.4
15	1000	22,500	84.9	23.2
10	1700	10,067	53.8	14.7
15	1700	15,100	67.5	18.5

6 Determination of the Heat Flux Uncertainty

6.1 Schmidt-Boelter Type Heat Flux Gage – Net Flux Uncertainty

Examples of commercially available heat flux gages are Gardon, Schmidt-Boelter, thin-film, and thermopile types. In all of these gages, an electrical output is generated from differential TCs or thermopiles.

By calibrating the gage in a blackbody furnace, one can obtain a radiation calibration factor, normally assumed to be linear with applied flux, so one can convert the voltage output to a corresponding net or incident flux. In such furnaces convection is assumed to be negligible because design tradeoffs are made to reduce convective effects. Typical calibration factors are in flux per milli-volt (e.g., xxx kW/m²/mV). In a purely radiative environment, one can estimate the incident radiative flux by knowing the sensing surface absorptivity and assuming the gage surface temperature is low enough so the emitted flux is negligible.

As stated earlier, comparing to a calibration gage (e.g., a radiometer), one can directly obtain an incident heat flux calibration. This type of calibration is only accurate for applications with negligible convection or for gages with equivalent response for radiation and convection. For this application (hydrocarbon fuel fires), the total heat flux has both components, so we desire the net flux calibration to both radiation and convection.

If the heat source is purely convective, then conversion from voltage output to flux is made via a convective calibration factor. The radiative and convective calibration factors may not be equal, and convective calibration factors may not be available, depending on the manufacturer's calibration capabilities. Should the heat source be part radiative and part convective (as in a hydrocarbon fuel fire), one needs to know the fractions of each and the calibration factor for each type of heat transfer to accurately estimate the incident heat flux.

Alternatively, one can obtain a correction factor for various gage sizes and convective HTC's (similar to what Kuo and Kulkarni (ref [9]) did for Gardon gages). The method detailed in the previous paragraph will be used here. The corrector factor method will be studied in future work.

The output of a typical gage is in the milli-volt (mV) range. Equation {14} shows the conversion from mV to flux.

$$q_{net} = K_{rad} * mV \quad [14]$$

Equation {14} has several limitations. One is the assumption that the source being measured is the same as the calibration source. As stated above, many calibration sources are only for radiative heat transfer, such as a blackbody cavity. In this case convection is assumed or made negligible and the calibration factor is for radiative flux only. Typical radiation calibration factor uncertainties are $\pm 3\%$ which includes the non-linearity of the gage calibration factor. If the gage is used in a purely radiative environment, an estimate of the net flux is accurate to about $\pm 3\%$ (assuming other uncertainty sources are negligible).

One may argue that equation {14} could also be written for a gage calibrated in "incident" flux mode. In this case the gage is calibrated to an incident heat flux source. If this is the case, the conversion from net to incident heat flux, and the associated uncertainties, is avoided (see equation {7}). However, the author believes the more physically realistic approach is to use net flux, as in equation {14}, because the gage physically responds only to the net flux absorbed into the sensing element. Unfortunately, this results in higher uncertainties, as will be seen later.

However, if the environment in which the gage is being used is not purely radiative, the conversion to heat flux is more complicated. Equation {15} expresses one method of converting to flux in an environment where convection is included.

$$q_{net} = mV * (K_{rad} * F_{rad} + K_{conv} * F_{conv}), \quad [15]$$

where F_{rad} is the fraction of radiative heat flux, F_{conv} is the convective fraction, and K_{rad} and K_{conv} are the radiative and convective calibration factors, respectively. This equation neglects non-linear effects, if they exist. Also, K_{conv} is often not a constant but is a function of the measurement environment (i.e., magnitude of and type of convection – i.e., shear flow or stagnation flow).

When the flux is purely radiative, $F_{rad} = 1$, $F_{conv} = 0$, the conversion to flux proceeds using the factory supplied (radiative only) calibration factor as in equation {14}. If one assumes the calibration factor is the same for convection and radiation, then equation {15} reduces to equation {14}. For all other cases equation {15} should be used.

There is evidence in the literature (e.g., refs. [9] and [10]) that the convective and radiative gage sensitivities are different for Gardon gages. Similarly, some evidence exists that the calibration factor for Schmidt-Boelter gages in purely radiative environments is different than for purely convective environments (ref. [8]). If this is the case, then one needs to determine the calibration factors for both radiative and convective environments, and know the fraction of the total flux that is both radiative and convective, in order to obtain an accurate estimate of the net flux to the sensing

surface. In practical terms, the parameters in equation {15} (except K_{rad} and mV) are often poorly known.

One S-B gage calibrated using a blackbody cavity (purely radiative) had a calibration factor of approximately $12.8 \text{ kW/m}^2/\text{mV}$.⁶ The same gage was calibrated in a purely convective environment and the calibration factor was as high as about $18.2 \text{ kW/m}^2/\text{mV}$ for large convective heat transfer coefficients (e.g., $600 \text{ W/m}^2\text{-K}$) or about 29% larger than the radiative-only calibration factor (ref. [8]). When the convective coefficients were less than $100 \text{ W/m}^2\text{-K}$, as is the case for a 30 cm diameter cylinder in a fire (see Tables 4 & 5), the calibration factor dropped to an extrapolated ($h=0$) value of about $14.4 \text{ kW/m}^2/\text{mV}$, or about 12% greater than the radiative-only calibration factor ($12.8 \text{ kW/m}^2/\text{mV}$). Linearly extrapolating, the calibration factor for $20 < h < 30$ is about $15.4 \text{ kW/m}^2/\text{mV}$, slightly higher than the 14.4 value. In this study it will be assumed that the calibration factors are 12.8 and $15.4 \text{ kW/m}^2/\text{mV}$ for K_{rad} and K_{conv} , respectively. The manufacturer provides an accuracy of $\pm 3\%$ for the gage, and that will be assumed to be the uncertainty of the calibration factor K_{rad} . K_{conv} is not known precisely, so the uncertainty in K_{conv} (ΔK_{conv}) will be assumed to be $\pm 20\%$ based on engineering judgment.⁷

For a water-cooled gage, the sensing surface temperature is relatively constant, assumed to be the cooling water temperature. In this case the surface temperature (T_s) is assumed to be 300 K .

The same methodology used in equation {5} will be used to estimate the uncertainty in net flux using an S-B heat flux gage. Determining the sensitivity coefficients for equation {15} one obtains the following:

$$\begin{aligned} \partial q_{net} / \partial mV &= K_{rad} * F_{rad} + K_{conv} * F_{conv} \\ \partial q_{net} / \partial K_{rad} &= mV * F_{rad} \\ \partial q_{net} / \partial F_{rad} &= mV * K_{rad} \\ \partial q_{net} / \partial K_{conv} &= mV * F_{conv} \\ \partial q_{net} / \partial F_{conv} &= mV * K_{conv} \end{aligned} \quad \{16\}$$

Therefore, the uncertainty in q_{net} , Δq_{net} , is estimated as follows:

$$\Delta q_{net} = \{((K_{rad} * F_{rad} + K_{conv} * F_{conv}) * \Delta mV)^2 + ((mV * F_{rad}) * \Delta K_{rad})^2 + ((mV * K_{rad}) * \Delta F_{rad})^2 + ((mV * F_{conv}) * \Delta K_{conv})^2 + ((mV * K_{conv}) * \Delta F_{conv})^2\}^{1/2} \quad \{17\}$$

The total uncertainty of net flux will be evaluated in a typical fire, assuming that the gage calibration factors do not change (i.e., the gage does not foul because of soot deposition) and the gage surface temperature does not change (i.e., the water cooling is effective). The parameters shown in Table 6 are assumed to be relevant for this case.

⁶ Medtherm Corp., Model #96-15T-15RB.

⁷ Author's note: It is planned that Dr. Tom Diller, Virginia Tech Univ., will be performing additional convective calibrations of several Schmidt-Boelter (Medtherm) gages in 2006. Results of those calibrations may be different than those reported here. We expect to publish those results as they become available.

Table 6: Parameters and Parameter Uncertainties for Use in Low Wind Case (100 kW/m² net flux)

Parameter	Value	Comments and Source of Information
K_{rad}	12.8 kW/m ² /mV	Medtherm Corp. calibration
ΔK_{rad}	± 0.4 kW/m ² /mV	$\pm 3\%$ uncertainty from manufacturer's specs.
K_{conv}	15.4 kW/m ² /mV	Dr. Diller's data
ΔK_{conv}	± 3.1 kW/m ² /mV	$\pm 20\%$ assumed uncertainty
F_{rad}	0.80	Engineering judgment
ΔF_{rad}	± 0.16	Engineering judgment; 20%, see end of Section 5.4
F_{conv}	0.20	Engineering judgment
ΔF_{conv}	± 0.16	Based on ΔF_{rad}
mV	7.81 mV	Based on total flux of about 100 kW/m ² and cal factor of 12.8 kW/m ² /mV
ΔmV	± 0.078 mV	1% (ref. [26])

Substituting the values from Table 6 into equation {17} one obtains an estimate for each of the terms:

$$\begin{aligned}
 ((K_{rad} * F_{rad} + K_{conv} * F_{conv}) * \Delta mV)^2 &= 1.0 \\
 (mV * F_{rad} * \Delta K_{rad})^2 &= 6.3 \\
 (mV * K_{rad} * \Delta F_{rad})^2 &= 255.8 \\
 (mV * F_{conv} * \Delta K_{conv})^2 &= 23.4 \\
 (mV * K_{conv} * \Delta F_{conv})^2 &= 370.3
 \end{aligned}
 \tag{18}$$

Substituting each of the terms into equation {17}, the net flux uncertainty is about 25.6 kW/m², or about 25.6% of the assumed total of 100 kW/m². In equation {18} it is evident that the 3rd and 5th terms dominate. In those terms, the large uncertainties in the fractions of radiative and convective flux contribute to the large overall uncertainties.

As a check on the analysis, one can estimate the uncertainty in a purely radiative environment. The result should be the manufacturer's reported value of $\pm 3\%$. If one assumes negligible convective flux, then $F_{conv} = 0$ (same for ΔF_{rad} and ΔF_{conv}), so the last 3 terms in equation {17} are zero; therefore, equation {17} reduces to the following:

$$\Delta q_{net} = \{(K_{rad} * \Delta mV)^2 + (mV * \Delta K_{rad})^2\}^{1/2}.
 \tag{19}$$

Substituting values into equation {19} the uncertainty is about 3.3 kW/m², or about 3.3%. This would be expected because the main source of uncertainty is the $\pm 3\%$ uncertainty in K_{rad} reported by the manufacturer.

A similar analysis has been performed for the high wind case. Table 7 shows the parameters used. For this case the total uncertainty is estimated to be 56.1 kW/m², or about 14.6% of the total.

Table 7: Parameters and Parameter Uncertainties for Use in High Wind Case

Parameter	Value	Comments and Source of Information
K_{rad}	12.8 kW/m ² /mV	Medtherm Corp. calibration
ΔK_{rad}	± 0.4 kW/m ² /mV	$\pm 3\%$ uncertainty from manufacturer's specs.
K_{conv}	15.4 kW/m ² /mV	Dr. Diller's data
ΔK_{conv}	± 3.1 kW/m ² /mV	$\pm 20\%$ assumed uncertainty
F_{rad}	0.90	Engineering judgment
ΔF_{rad}	± 0.09	Engineering judgment; 10%, see end of Section 5.4
F_{conv}	0.10	Engineering judgment
ΔF_{conv}	± 0.09	Based on ΔF_{rad}
mV	30.00 mV	Based on total flux of about 383 kW/m ² and cal factor of 12.8 kW/m ² /mV
ΔmV	$\pm .300$ mV	1% (see ref. [26])

In summary, it will be assumed that the net flux uncertainty for S-B type gages is about $\pm 25\%$ for the case of a mixed radiation/convection environment in low winds, and $\pm 15\%$ for high winds.

6.2 Calorimeter and Inverse Heat Conduction Method – Net Flux Uncertainty

As stated above, there are some applications where commercially available gages don't function well, for example in sooty environments. In these cases an inverse heat conduction method can be used to infer the net flux into the heated surface. By measuring temperature at a surface, knowing material properties, and establishing a well known boundary condition on the unheated side one can use an inverse heat conduction code to estimate the net heat flux. Figure 2 shows such a configuration. This device will be called a "calorimeter."

Referring to Figure 2, one can see that at the sensing surface, the energy balance is the same as in Figure 1. On the calorimeter, the sensing element is the TC and is mounted on the unheated side of the surface. The insulation surface farthest from the heated side is assumed to be adiabatic, or its temperature is measured to provide a prescribed temperature boundary condition. The insulation temperature measurement can be made and substituted for the adiabatic condition,

but this is not required. The TC could be mounted on the heated surface but unheated side measurements are normally made because this measurement is believed to be more accurate.

The temperature measurements, the geometry, and material properties of the sensing surface (normally stainless steel) and the insulation as functions of temperature are used with a 1-dimensional inverse heat conduction program to estimate the net flux into the surface. This is a convenient method because one does not need to know the radiation and convective calibration sensitivities and fractions to estimate the net flux. Whatever is net into the heated surface of the calorimeter is sensed by the TC, and converted to a flux using an inverse heat conduction program. Drawbacks are that there is no way to estimate the radiative and convective contributions, except via a model, and the transient response is poor.

As indicated earlier, two codes typical of those in use are SODDIT (Sandia One-Dimensional Direct and Inverse Thermal) and IHCP1D (Inverse Heat Conduction Program 1-Dimensional) (see refs. [1] and [2]).

Estimating the uncertainty of the net flux using an inverse method (IHCP1D) has been performed by Figueroa, et al. (ref. [3]). Typical values of uncertainty were $\pm 15\text{-}19\%$ with 95% confidence at peak fluxes. Uncertainties at early and late times are larger because the nominal net flux at those times is small. For ease of calculation, it will be assumed that the maximum net flux uncertainty is $\pm 20\%$.

6.3 Energy Balance Method – Incident Heat Flux Uncertainty

6.3.1 Thin Plate Gage Background

A thin plate gage has been used as a heat flux gage in several fire applications (ref. [27]). In this method the transient temperature of a thin metal plate is measured by a TC. The back side of the plate is insulated to obtain a known boundary condition; the plate is thin enough that there is negligible temperature difference through the thickness. It is also assumed that the heat transfer is 1-dimensional. The gage is analyzed by first establishing a control volume on the plate surface exposed to the fire. In ref. [5] the thin film gage is called the Sandia Heat Flux Gage (HFG). An energy balance is written similar to equation {3}. The incident radiative flux is written as follows:

$$q_{inc,r} = \sigma T_s^4 + (h/\varepsilon)(T_s - T_\infty) + q_{steel}/\varepsilon + q_{ins}/\varepsilon . \quad \{20\}$$

If one compares equations {3} and {20}, the net flux may be written as follows:

$$q_{abs} = q_{steel} + q_{insul} , \quad \{21\}$$

where q_{steel} is the sensible heat stored in the thin plate, and q_{insul} is the heat loss into the insulation. Even though the insulation has a low conductivity, there is still heat loss and that has to be accounted for in the model.

The sensible heat stored in the thin plate is evaluated as follows:

$$q_{steel}(t) = (\rho c_p L)(dT_{plate} / dt) \quad \{22\}$$

where ρ is the plate density, c_p the specific heat, and L the plate thickness.

The heat loss into the insulation is evaluated as follows:

$$q_{ins}(t) = k_{ins}(\partial T_{ins}(z,t) / \partial z) \quad \{23\}$$

where z is the direction perpendicular to the plane of the plate.

The data reduction equation used is as follows:

$$q_{inc,r} = \sigma T_s^4 + (h / \varepsilon)(T_s - T_\infty) + (\rho c_p L / \varepsilon)(\partial T_s / \partial t) + (k_{ins} / \varepsilon)(\partial T_{ins} / \partial z). \quad \{24\}$$

Using a finite difference expression for equation {24}, the authors solve for the incident heat flux by use of the thermal and geometric properties of the plate and insulation, the plate temperature, convective heat transfer coefficient, and the free stream gas temperature. Benefits of this method are relative simplicity, independence from the type of heat transfer (radiative or convective), and the gage does not need to be calibrated. On the negative side one needs good estimates for all the input parameters in equation {24}, and the transient response is poor. Output is in incident heat flux, not net.

The terms in equations {24} were evaluated (ref. [5]) so their relative importance could be determined. However, the application was calibration inside a cylindrical steel tube (not a fire) so only natural convection was present. Figure 12 of the reference shows the results for a step increase in flux. It was shown that during the *early* portion of the transient the order of importance of each of the terms in equation {24} was as follows: 1) the sensible heat stored in the plate; 2) the heat loss into the insulation; 3) the emitted flux; and 4) the convective flux. The convective flux was the least important in part because of the application (free convection in an enclosure). It would be more important in an open fire, where forced convection from the wind adds to the overall level of convection.

In the late portion of the transient and the steady portion the term of most importance was the emitted flux. All other terms were negligible. Therefore uncertainty in plate temperature is very important in the estimation of the flux in the late transient and steady portions.

The error caused by the relatively large TC attached to the thin plate is a large contributor to the large uncertainty at early times. Convective uncertainties and uncertainties in insulation properties are not large contributors.

$q_{inc,r}$ = incident radiative flux
 q_{emit} = emitted flux
 q_{conv} = convective flux
 q_{net} = net flux

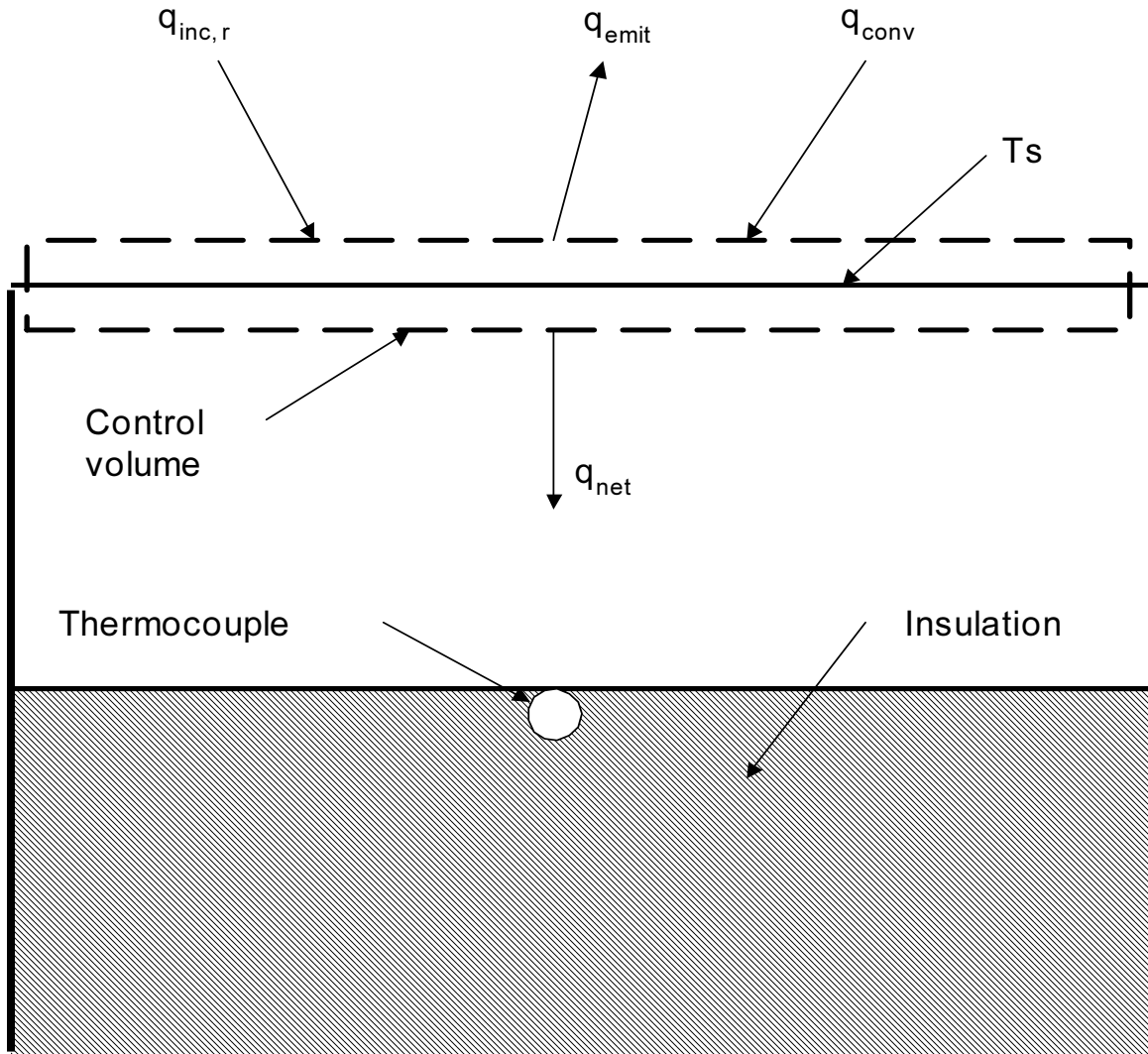


Figure 2 Calorimeter Details

A detailed uncertainty analysis was performed on the thin plate gage (i.e., the Sandia Heat Flux Gage [Sandia HFG]) and results are reported in ref. [5]. In that study the response of the Sandia HFG was compared to a water-cooled circular foil “Gardon” type heat flux gage. Uncertainty sources were separated into three categories: 1) simplifying assumptions; 2) uncontrolled variabilities; and 3) “missing physics.” Examples of simplifying assumptions are negligible

temperature gradient in the plate and 1-dimensional conduction. Examples of uncontrolled variability are uncertainties in material properties, geometric dimensions, TC uncertainty, etc. Missing physics include “phenomena commonly buried under empirical constants that are created to bring the modeled instrument response into agreement with the observed experimental response to a known input” (ref. [5]). One example is the effect of a finite sized TC on the thin plate temperature – the plate temperature will be lower due to the presence of the TC.

Figure 19 of the reference shows a plot of the three uncertainty sources as a function of time. In the transient portion of the test, when the flux increased from zero to the steady value, missing physics and uncontrolled variability were the largest contributors, while during the steady portion simplifying assumptions and uncontrolled variability were the most important.

Because the TC used was large (0.063” diameter) as compared with the plate thickness (0.010”), the TC likely has enough thermal mass to depress the plate temperature, causing the thin plate flux to lag behind the Gardon gage flux. For robustness, 0.063 inch diameter mineral-insulated, metal-sheathed TCs are typically used. However, these TCs have a time constant of about 3 sec in air, so rapid flux changes are not accurately captured.

Figure 15 in ref. [5] provides uncertainty estimates for the HFG during the transient and steady portions of the test. For a step input in flux of about 100 kW/m², the agreement between the two gages was very good in the steady portion, but poor in the transient. During the steady portion the uncertainty is about ±8% of the nominal value of 100 kW/m². The values of the Gardon and thin plate gages are almost coincident. However, during the transient portion the thin plate gage lags behind the Gardon so much so that even with the estimated uncertainty bounds, the thin plate response does not approach the Gardon gage response. Therefore, for steady applications the thin plate (Sandia HFG) works well, but for transient cases it lags far behind the Gardon gage.

6.3.2 Thin Plate Gage Applied to Calm and Windy Fires

To estimate the uncertainty in incident heat flux when using the thin plate/energy balance method for fires, the same procedure is used on equation {24} as was used on equation {3}:

$$\Delta q_{inc,r} = [((\partial q_{inc,r} / \partial T_s) \Delta T_s)^2 + ((\partial q_{inc,r} / \partial \varepsilon) \Delta \varepsilon)^2 + \dots]^{1/2}. \quad \{25\}$$

Evaluating the sensitivity coefficients one obtains the following:

$$\begin{aligned}
\partial q_{inc,r} / \partial h &= (T_s - T_\infty) / \varepsilon \\
\partial q_{inc,r} / \partial \varepsilon &= -(h / \varepsilon^2)(T_s - T_\infty) - [(\rho c L) / \varepsilon^2] \partial T_s / \partial t - (k_{ins} / \varepsilon^2) \partial T_{ins} / \partial z \\
\partial q_{inc,r} / \partial T_s &= 4\sigma T_s^3 + h / \varepsilon \\
\partial q_{inc,r} / \partial \rho c_p &= (L / \varepsilon) \partial T_s / \partial t \\
\partial q_{inc,r} / \partial L &= (\rho c_p / \varepsilon) \partial T_s / \partial t \\
\partial q_{inc,r} / \partial k_{ins} &= (1 / \varepsilon) \partial T_{ins} / \partial z \\
\partial q_{inc,r} / \partial T_\infty &= -h / \varepsilon \\
\partial q_{inc,r} / \partial T_{s,t} &= \rho c_p L / \varepsilon \\
\partial q_{inc,r} / \partial T_{ins,z} &= k_{ins} / \varepsilon
\end{aligned} \tag{26}$$

where “ $T_{s,t}$ ” is the partial derivative of the steel surface temperature with respect to time ($\partial T_s / \partial t$) and “ $T_{ins,z}$ ” is the partial derivative of the insulation temperature with respect to the z-direction ($\partial T_{ins} / \partial z$).

Geometric and thermal properties are defined in ref. [5] as follows:

- L = thin plate thickness = 0.010” = 0.0254 cm,
- ρc_p = plate density*specific heat = $1925.4 + 9.418 * T - 0.013641 * T^2 + 9.441096 \times 10^{-6} * T^3 - 2.34159 \times 10^{-9} * T^4$ (kJ/m³-K), temperature in K⁸,
- ε = surface emissivity of plate = 0.85,
- h = convective heat transfer coefficient = 0.021 kW/m²-K for low wind case, and 0.031 kW/m²-K for high wind case,
- k_{ins} = insulation thermal conductivity = $-6.05 \times 10^{-3} + 6.98 \times 10^{-5} * T + 1.04 \times 10^{-7} * T^2$ (W/m-K),
- $T_{s,t} = \partial T_s / \partial t$ = change in plate surface temperature with respect to time. This term is large during the early portion of the fire when the plate is heating up, but small at late times because the plate temperature has roughly equilibrated with the fire. This term will be evaluated in the examples.
- $T_{ins,z} = \partial T_{ins} / \partial z$ = gradient through the insulation near the steel-insulation interface. This gradient is low during the early period, rises to a peak during the intermediate period, and slowly drops at late times. This term will also be evaluated in the examples.

⁸ Personal communication, L.L. Humphries, Analysis & Modeling Department 6862, February 2, 2005.

7 Examples

Several examples provide uncertainty estimates for incident radiative heat flux. These correspond to the early phase of a fire when the gage is close to the initial temperature, late when the gage is close to the fire temperature, and an intermediate time when the gage temperature is between the extremes. Examples will be analyzed for the S-B type gage, the calorimeter, and the thin plate in low wind and high wind fires. It is assumed that the fire is not affected by the presence of the gage, therefore the incident flux is constant at 92 kW/m² for the low wind case and 400 kW/m² for the high wind case.

7.1 S-B Type Gage

7.1.1 Low Wind Case

7.1.1.1 Early Times

To determine the uncertainty in incident heat flux, one has to evaluate the parameters in equation {7}, reproduced below for convenience:

$$\Delta q_{inc,r} = [(\Delta q_{net} / \varepsilon)^2 + (((-q_{net} / \varepsilon^2) + (h / \varepsilon^2)(T_{\infty} - T_s))\Delta\varepsilon)^2 + ((4\sigma T_s^3 + h / \varepsilon)\Delta T_s)^2 + ((-1 / \varepsilon)(T_{\infty} - T_s)\Delta h)^2 + ((-h / \varepsilon)\Delta T_{\infty})^2]^{1/2} \quad \{7\}$$

Values shown in Table 8 are used for this case (S-B gage, early times, low wind). The net flux into the gage surface is assumed to be 100 kW/m². The net flux uncertainty is assumed to be $\pm 25\%$, as estimated in Section 6.1. Gage surface emissivity is assumed to be typical of Pyromark black paint. The emissivity was measured as 0.85 ± 0.09 emissivity units (ref. [19]). The maximum value of the convective heat transfer coefficient (HTC) is taken from Table 4, 21 W/m²-K. Because this is not known to high accuracy, a $\pm 50\%$ uncertainty will be assumed. The surface temperature, in this case the S-B gage sensing surface temperature, is assumed to be a constant value of 300 K because the gage is water-cooled. Uncertainty in that value is low, assumed to be $\pm 5\%$. The free stream gas temperature is assumed to be 1300 K with relatively large variations of ± 325 K ($\pm 25\%$) due to the turbulent nature of the fire.

Table 8: Parameter Values for the S-B Gage, Early Times, Low Wind Fire

Parameter	Value	Comments
q_{net}	100 kW/m ²	Total of radiative and convective parts
Δq_{net}	± 25 kW/m ²	$\pm 25\%$ from above
ε	0.85	Pyromark paint emissivity
$\Delta\varepsilon$	± 0.09	10% uncertainty from measurements (ref. [19])
h	0.021 kW/m ² -K	Maximum value from Table 4
Δh	± 0.010 kW/m ² -K	50% uncertainty
T_s	300 K	Water-cooled gage, constant surface temperature
ΔT_s	± 15 K	Assume 5% uncertainty
T_∞	1300 K	Free stream gas temperature
ΔT_∞	± 325 K	Assumed variation in free stream gas temperature, $\pm 25\%$

Each one of the terms in equation {7} was evaluated separately. Results are shown below.

$$\begin{aligned}
 (\Delta q_{net} / \varepsilon)^2 &= 865.1 \\
 (((-q_{net} / \varepsilon^2) - (h / \varepsilon^2)(T_\infty - T_s))\Delta\varepsilon)^2 &= 227.2 \\
 ((4\sigma T_s^3 + h / \varepsilon)\Delta T_s)^2 &= 0.2 \\
 ((1 / \varepsilon)(T_\infty - T_s)\Delta h)^2 &= 138.4 \\
 ((h / \varepsilon)\Delta T_\infty)^2 &= 64.5
 \end{aligned} \tag{27}$$

Combining the values in equation {27} into equation {7}, the total uncertainty in the incident flux is about 36.0 kW/m² and the incident radiative flux is 92 kW/m². Therefore, the total uncertainty in incident radiative flux is about $\pm 39\%$ of the total. This large uncertainty is a result, for the most part, of the large uncertainty in net flux and surface emissivity.

To determine the contribution of each of the uncertainty sources to the total uncertainty, the following procedure is used (ref. [28]). First, square equation {7}, then divide by the total incident flux uncertainty. The left side of the equation now equals 1.0. Each of the terms on the right side is also divided by the total uncertainty so the fraction of each term to the total can be evaluated. The result is:

$$\begin{aligned}
 \Delta q_{inc,r}^2 / \Delta q_{inc,r}^2 = 1.0 &= (-\Delta q_{net} / \varepsilon)^2 / \Delta q_{inc,r}^2 + (((-q_{net} / \varepsilon^2) + (h / \varepsilon^2)(T_\infty - T_s))\Delta\varepsilon)^2 / \Delta q_{inc,r}^2 \\
 + ((4\sigma T_s^3 + h / \varepsilon)\Delta T_s)^2 / \Delta q_{inc,r}^2 &+ ((1 / \varepsilon)(T_\infty - T_s)\Delta h)^2 / \Delta q_{inc,r}^2 + ((h / \varepsilon)\Delta T_\infty)^2 / \Delta q_{inc,r}^2
 \end{aligned} \tag{28}$$

Evaluation of each of the terms in equation {28} for the low wind case, early times, is provided in Table 9.

**Table 9: Relative Magnitude of Uncertainty Sources,
S-B Gage, Low Wind, Early Times**

Term	% of Total
$((\partial q_{inc,r} / \partial q_{abs}) * \Delta q_{abs})^2 / \Delta q_{inc,r}^2$	66.8
$((\partial q_{inc,r} / \partial \varepsilon) * \Delta \varepsilon)^2 / \Delta q_{inc,r}^2$	17.5
$((\partial q_{inc,r} / \partial T_s) * \Delta T_s)^2 / \Delta q_{inc,r}^2$	0
$((\partial q_{inc,r} / \partial h) * \Delta h)^2 / \Delta q_{inc,r}^2$	10.7
$((\partial q_{inc,r} / \partial T_\infty) \Delta T_\infty)^2 / \Delta q_{inc,r}^2$	5.0
All	100.0

It is evident from Table 9 that the largest contributors to the total uncertainty in incident radiative flux are the net flux, emissivity, and convective HTC uncertainties. The other two sources (uncertainty in gage surface temperature, and in gas free stream temperature) sum to less than about 5%.

7.1.1.2 Intermediate Times

Parameters for intermediate times for the S-B gage are the same as those for early times because the gage surface temperature is held constant by the water cooling and the convective HTC is virtually constant with surface temperature (see Table 4). Therefore, the flux uncertainty is the same, $\pm 39\%$.

7.1.1.3 Late Times

Parameters for late times for the S-B type gage are the same as those for early and intermediate times, therefore the flux uncertainty is the same, $\pm 39\%$.

7.1.2 High Wind Case

7.1.2.1 Early Times

For the high wind case the parameters are as shown in Table 10. Table 11 shows the contributions of each of the uncertainty sources to the total. The total uncertainty is approximately 90.8 kW/m². The incident radiative flux was assumed to be 400 kW/m² for this case, so the uncertainty in incident radiative flux is about $\pm 23\%$. From Table 11 the uncertainty in net flux is most important, followed by uncertainty in emissivity. All other sources sum to less than 11%.

7.1.2.2 Intermediate and Late Times

The total uncertainty is the same for intermediate and late times because parameters in Table 10 do not change.

Table 10: Parameter Values for Early Times, S-B Gage, High Wind Case

Parameter	Value	Comments
q_{net}	383 kW/m ²	Total of radiative and convective parts
Δq_{net}	± 57.5 kW/m ²	$\pm 15\%$ from discussion above
ε	0.85	Pyromark paint emissivity
$\Delta \varepsilon$	± 0.09	10% uncertainty from measurements (ref. [19])
h	0.031 kW/m ² -K	Maximum value from Table 5.
Δh	± 0.015 kW/m ² -K	50% uncertainty
T_s	300 K	Water-cooled gage
ΔT_s	± 15 K	Assume 5% uncertainty
T_∞	1700 K	Free stream gas temperature
ΔT_∞	± 425 K	Assumed variation in free stream gas temperature, $\pm 25\%$

Table 11: Relative Magnitude of Uncertainty Sources, S-B Gage, High Wind, Early Times

Term	% of Total
$((\partial q_{inc,r} / \partial q_{net}) * \Delta q_{net})^2 / \Delta q_{inc,r}^2$	55.4
$((\partial q_{inc,r} / \partial \varepsilon) * \Delta \varepsilon)^2 / \Delta q_{inc,r}^2$	34.2
$((\partial q_{inc,r} / \partial T_s) * \Delta T_s)^2 / \Delta q_{inc,r}^2$	0.0
$((\partial q_{inc,r} / \partial h) * \Delta h)^2 / \Delta q_{inc,r}^2$	7.4
$((\partial q_{inc,r} / \partial T_\infty) \Delta T_\infty)^2 / \Delta q_{inc,r}^2$	3.0
All	100.0

7.2 Calorimeter and Inverse Heat Conduction Method

7.2.1 Low Wind Case

7.2.1.1 Early Times

In this case the values in Table 8 also apply to the calorimeter, except for the uncertainty in net flux. The net flux uncertainty is assumed to be $\pm 20\%$, as stated above. The emissivity, heat transfer coefficient, and free stream gas temperature, as well as their respective uncertainties, are the same as in Table 8. The sensing surface temperature of the calorimeter is also the same but for a different reason. The S-B gage surface is water-cooled to maintain at that temperature (300

K), while the calorimeter surface begins at 300 K but rises in time. For early times the calorimeter surface will also be assumed to be 300 K.

In a manner similar to the S-B calculations, values in equation {7} were estimated. The result is a total uncertainty of 31.4 kW/m², which is 34.1% of the total of the 92 kW/m² incident radiative flux. Table 12 shows the relative importance of each of the uncertainty sources. The most important are the uncertainty in net flux, then the surface emissivity, and the convective heat transfer coefficient.

**Table 12: Relative Magnitude of Uncertainty Sources,
Calorimeter/Inverse Heat Conduction Method, Low Wind, Early Times**

Term	% of Total
$((\partial q_{inc,r} / \partial q_{net}) * \Delta q_{net})^2 / \Delta q_{inc,r}^2$	56.3
$((\partial q_{inc,r} / \partial \varepsilon) * \Delta \varepsilon)^2 / \Delta q_{inc,r}^2$	23.1
$((\partial q_{inc,r} / \partial T_s) * \Delta T_s)^2 / \Delta q_{inc,r}^2$	0.0
$((\partial q_{inc,r} / \partial h) * \Delta h)^2 / \Delta q_{inc,r}^2$	14.1
$((\partial q_{inc,r} / \partial T_\infty) \Delta T_\infty)^2 / \Delta q_{inc,r}^2$	6.6
All	100.0

7.2.1.2 Intermediate Times

The parameters in Table 13 are assumed for intermediate times. The net flux is lower because the surface is at a higher temperature, so the surface emission is higher. The convective HTC is the same because the surface temperature has only a small effect. The surface temperature of the calorimeter has risen from 300 K to 800 K. Table 14 shows the relative magnitude of each of the uncertainty sources.

The total uncertainty is approximately 24.7 kW/m², or about 27% of the total incident radiative flux. The uncertainty in net flux is the largest contributor, followed by the emissivity, and then the free stream gas temperature.

Table 13: Parameter Values for Intermediate Times, Calorimeter, Low Wind Case

Parameter	Value	Comments
q_{net}	80 kW/m ²	Total of radiative and convective parts
Δq_{net}	±16 kW/m ²	±20% from above
ε	0.85	Pyromark paint emissivity
$\Delta\varepsilon$	±0.09	10% uncertainty from measurements (ref. [19])
h	0.021 kW/m ² -K	Maximum value from Table 4.
Δh	±0.010 kW/m ² -K	50% uncertainty
T_s	800 K	Surface temperature above ambient
ΔT_s	±40 K	Assume 5% uncertainty
T_∞	1300 K	Free stream gas temperature
ΔT_∞	±325 K	Assumed variation in free stream gas temperature, ±25%

Table 14 Relative Magnitude of Uncertainty Sources, Calorimeter/Inverse Heat Conduction Method, Low Wind, Intermediate Times

Term	% of Total
$((\partial q_{inc,r} / \partial q_{abs}) * \Delta q_{abs})^2 / \Delta q_{inc,r}^2$	57.9
$((\partial q_{inc,r} / \partial \varepsilon) * \Delta \varepsilon)^2 / \Delta q_{inc,r}^2$	20.8
$((\partial q_{inc,r} / \partial T_s) * \Delta T_s)^2 / \Delta q_{inc,r}^2$	5.2
$((\partial q_{inc,r} / \partial h) * \Delta h)^2 / \Delta q_{inc,r}^2$	5.7
$((\partial q_{inc,r} / \partial T_\infty) \Delta T_\infty)^2 / \Delta q_{inc,r}^2$	10.5
All	100.0

7.2.1.3 Late Times

The surface temperature of the calorimeter rises during the fire. At late times, the surface comes to equilibrium with the fire, so the net flux is negligible. The surface temperature is equivalent to the effective “flame” temperature of the surrounding environment. This may or may not be equal to the gas temperature, but it can be assumed to be the same so the convective component will be assumed negligible. Table 15 shows the assumed values for the calorimeter late in the fire.

Table 15 Parameter Values for Late Times, Calorimeter, Low Wind Case

Parameter	Value	Comments
q_{net}	0 kW/m ²	When calorimeter reaches a steady value, the total net flux goes to zero.
Δq_{net}	±10 kW/m ²	Large uncertainty at low flux levels. This is an approximation.
ϵ	0.85	Pyromark paint emissivity
$\Delta\epsilon$	±0.09	10% uncertainty from measurements (ref. [19])
h	0.021 kW/m ² -K	Maximum value from Table 4.
Δh	±0.010 kW/m ² -K	50% uncertainty
T_s	1300 K	Surface temperature in equilibrium with fire
ΔT_s	±65 K	Assume 5% uncertainty
T_∞	1300 K	Free stream gas temperature
ΔT_∞	±325 K	Assumed variation in free stream gas temperature, ±25%

Table 16: Relative Magnitude of Uncertainty Sources, Calorimeter/Inverse Heat Conduction Method, Low Wind, Late Times

Term	% of Total
$((\partial q_{inc,r} / \partial q_{net}) * \Delta q_{net})^2 / \Delta q_{inc,r}^2$	10.2
$((\partial q_{inc,r} / \partial \epsilon) * \Delta \epsilon)^2 / \Delta q_{inc,r}^2$	0.0
$((\partial q_{inc,r} / \partial T_s) * \Delta T_s)^2 / \Delta q_{inc,r}^2$	85.1
$((\partial q_{inc,r} / \partial h) * \Delta h)^2 / \Delta q_{inc,r}^2$	0.0
$((\partial q_{inc,r} / \partial T_\infty) \Delta T_\infty)^2 / \Delta q_{inc,r}^2$	4.7
All	100.0

The total uncertainty is approximately 36.9 kW/m², or about ±40% of the total. This case is very different from the early time case. The surface temperature term contributes the majority of the uncertainty, as shown in Table 16. Accurate flux measurements at late times using a calorimeter are only possible with accurate surface temperature measurements.

7.2.2 High Wind Case

7.2.2.1 Early Times

Values in Table 17 apply to the calorimeter for early times in high winds. The net flux uncertainty is assumed to be $\pm 20\%$ and the nominal net flux is 383 kW/m^2 . The emissivity, heat transfer coefficient, and free stream gas temperature, as well as their respective uncertainties, are the same as for the S-B gage.

Table 17: Parameter Values for the Calorimeter, High Wind Case, Early Times

Parameter	Value	Comments
q_{net}	383 kW/m^2	Total of radiative and convective parts
Δq_{net}	$\pm 76.6 \text{ kW/m}^2$	$\pm 20\%$
ϵ	0.85	Pyromark paint emissivity
$\Delta \epsilon$	± 0.09	10% uncertainty from measurements (ref. [19])
h	$0.031 \text{ kW/m}^2\text{-K}$	Assume velocity is 5 m/s, corresponding to object 2 m above fire base.
Δh	$\pm 0.015 \text{ kW/m}^2\text{-K}$	50% uncertainty
T_s	300 K	Surface temperature at ambient
ΔT_s	$\pm 15 \text{ K}$	Assume 5% uncertainty
T_∞	1700 K	Free stream gas temperature
ΔT_∞	$\pm 425 \text{ K}$	Assumed variation $\pm 25\%$

Evaluation results in a total uncertainty of 108.6 kW/m^2 , which is 27% of the total of the 400 kW/m^2 incident radiative flux. Table 18 shows the relative uncertainty of each of the uncertainty sources. In this case the net flux uncertainty is the dominant term, followed by the uncertainty in emissivity. Other terms are small.

Table 18: Relative Magnitude of Uncertainty Sources, Calorimeter/Inverse Heat Conduction Method, High Wind, Early Times

Term	% of Total
$((\partial q_{inc,r} / \partial q_{net}) * \Delta q_{net})^2 / \Delta q_{inc,r}^2$	68.9
$((\partial q_{inc,r} / \partial \epsilon) * \Delta \epsilon)^2 / \Delta q_{inc,r}^2$	23.9
$((\partial q_{inc,r} / \partial T_s) * \Delta T_s)^2 / \Delta q_{inc,r}^2$	0.0
$((\partial q_{inc,r} / \partial h) * \Delta h)^2 / \Delta q_{inc,r}^2$	5.2
$((\partial q_{inc,r} / \partial T_\infty) * \Delta T_\infty)^2 / \Delta q_{inc,r}^2$	2.0
All	100.0

7.2.2.2 Intermediate Times

The parameters in Table 19 are assumed for intermediate times. The net flux is lower because the surface is at a higher temperature. The surface temperature of the calorimeter has risen from 300 K to 800 K. Convection is lower because the temperature difference $T_{\infty}-T_s$ is less. The total uncertainty is about 101.2 kW/m², or about 25% of the total incident radiative flux. Table 20 shows that the net flux and emissivity uncertainties dominate, similar to early times.

Table 19: Parameter Values for the Calorimeter, Intermediate Times, High Winds

Parameter	Value	Comments
q_{net}	364 kW/m ²	Total of radiative and convective parts
Δq_{net}	± 72.7 kW/m ²	$\pm 20\%$ from above
ϵ	0.85	Pyromark paint emissivity
$\Delta \epsilon$	± 0.09	10% uncertainty from measurements (ref. [19])
h	0.031 kW/m ² -K	Maximum value from Table 5.
Δh	± 0.015 kW/m ² -K	50% uncertainty
T_s	800 K	Surface temperature rises above ambient
ΔT_s	± 40 K	Assume 5% uncertainty
T_{∞}	1700 K	Free stream gas temperature
ΔT_{∞}	± 425 K	Assumed variation gas temperature, $\pm 25\%$

Table 20: Relative Magnitude of Uncertainty Sources, Calorimeter/Inverse Heat Conduction Method, High Wind, Intermediate Times

Term	% of Total
$((\partial q_{inc,r} / \partial q_{net}) * \Delta q_{net})^2 / \Delta q_{inc,r}^2$	71.6
$((\partial q_{inc,r} / \partial \epsilon) * \Delta \epsilon)^2 / \Delta q_{inc,r}^2$	23.3
$((\partial q_{inc,r} / \partial T_s) * \Delta T_s)^2 / \Delta q_{inc,r}^2$	0.4
$((\partial q_{inc,r} / \partial h) * \Delta h)^2 / \Delta q_{inc,r}^2$	2.5
$((\partial q_{inc,r} / \partial T_{\infty}) * \Delta T_{\infty})^2 / \Delta q_{inc,r}^2$	2.2
All	100.0

7.2.3 Late Times

At late times, the surface comes to equilibrium with the fire, so the net flux is negligible. The surface temperature is equivalent to the effective “flame” temperature of the surrounding environment. This is assumed to be close to the gas temperature, so the convective component is assumed negligible. Table 21 shows the assumed values for the calorimeter late in the fire.

Table 21: Parameter Values for Late Times, Calorimeter, High Wind Case

Parameter	Value	Comments
q_{net}	0 kW/m ²	When calorimeter reaches a steady value, the total net flux goes to zero.
Δq_{net}	±10 kW/m ²	Large uncertainty at low flux levels. This is an approximation.
ϵ	0.85	Pyromark paint emissivity
$\Delta\epsilon$	±0.09	10% uncertainty from measurements (ref. [19])
h	0.031 kW/m ² -K	Maximum value from Table 5.
Δh	±0.015 kW/m ² -K	50% uncertainty
T_s	1700 K	Surface temperature in equilibrium with fire.
ΔT_s	±85 K	Assume 5% uncertainty
T_∞	1700 K	Free stream gas temperature
ΔT_∞	±425 K	Assumed variation in gas temperature, ±25%

The total flux uncertainty is approximately 99.7 kW/m² or about 25% of the total. This case is similar to the low wind, late time case. The third term (surface temperature uncertainty) contributes almost all to the total, as shown in Table 22.

Table 22: Relative Magnitude of Uncertainty Sources, Calorimeter/Inverse Heat Conduction Method, High Wind, Late Times

Term	% of Total
$((\partial q_{inc,r} / \partial q_{net}) * \Delta q_{net})^2 / \Delta q_{inc,r}^2$	1.4
$((\partial q_{inc,r} / \partial \epsilon) * \Delta \epsilon)^2 / \Delta q_{inc,r}^2$	0.0
$((\partial q_{inc,r} / \partial T_s) * \Delta T_s)^2 / \Delta q_{inc,r}^2$	96.2
$((\partial q_{inc,r} / \partial h) * \Delta h)^2 / \Delta q_{inc,r}^2$	0.0
$((\partial q_{inc,r} / \partial T_\infty) \Delta T_\infty)^2 / \Delta q_{inc,r}^2$	2.4
All	100.0

7.3 Energy Balance Method/Thin Plate Gage

This section evaluates the incident heat flux uncertainty when using the energy balance method. This case is different from the other two in that net heat flux is not directly estimated. The energy stored in the plate and energy loss into the insulation replaces the net flux.

Referring to Section 6.3.2, the following terms have to be evaluated:

$$\begin{aligned}
 \partial q_{inc,r} / \partial h &= (T_s - T_\infty) / \varepsilon \\
 \partial q_{inc,r} / \partial \varepsilon &= -(h / \varepsilon^2)(T_s - T_\infty) - [(\rho c L) / \varepsilon^2] \partial T_s / \partial t - (k_{ins} / \varepsilon^2) \partial T_{ins} / \partial z \\
 \partial q_{inc,r} / \partial T_s &= 4\sigma T_s^3 + h / \varepsilon \\
 \partial q_{inc,r} / \partial \rho c_p &= (L / \varepsilon) \partial T_s / \partial t \\
 \partial q_{inc,r} / \partial L &= (\rho c_p / \varepsilon) \partial T_s / \partial t \\
 \partial q_{inc,r} / \partial k_{ins} &= (1 / \varepsilon) \partial T_{ins} / \partial z \\
 \partial q_{inc,r} / \partial T_\infty &= -h / \varepsilon \\
 \partial q_{inc,r} / \partial T_{s,t} &= \rho c_p L / \varepsilon \\
 \partial q_{inc,r} / \partial T_{ins,z} &= k_{ins} / \varepsilon
 \end{aligned} \tag{29}$$

7.3.1 Low Wind Fire

7.3.1.1 Early Times

Table 23 provides estimates for the parameters in equation {29} at early times. Parameters in Table 23 were obtained from Table 8 (emissivity, convective HTC, surface temperature, and gas temperature), from ref. [5] (ρc_p , L , k_{ins} , $T_{s,t}$, and $T_{ins,z}$), and ref. [3] (ΔL).

Values were substituted into equation {29} and the uncertainty estimated. The total uncertainty for the thin plate/energy balance method, low wind case, early times, is about 29.3 kW/m², or about $\pm 32\%$ of the total incident radiative value. Table 24 shows the relative contributions of each of the terms. In contrast to the S-B gage or calorimeter/inverse heat conduction method, the surface emissivity is only a small uncertainty source. The temporal gradient of the surface temperature ($\partial T_s / \partial t$) is by far the most important uncertainty source. Other important sources are the convective heat transfer coefficient and the free stream temperature. Other sources are almost negligible.

The emissivity is less of a contributor for the thin plate gage because the terms containing $\Delta \varepsilon$ (energy stored in plate and insulation loss term) are smaller contributors as compared with q_{net} , which is a large uncertainty source for the calorimeter and S-B gage.

Of note is that the spatial gradient in the insulation is of minor importance. A large uncertainty ($\pm 50\%$) was assumed in Table 23 to see what the effect would be on the total uncertainty. Even with this large value the effect on the total was negligible (see Table 24).

Data were analyzed from two previous experiments performed in a 26 ft diameter open pool. A number of thin plate heat flux gages (i.e., the Sandia HFGs) were placed at the pool surface to measure the heat flux to the pool surface. Data from all the gages were used to estimate the temporal gradient of the surface temperature during the fire. Results from one test are shown in Figure 3. The temporal gradient is a maximum (40°C/s) at early times, and drops to an average of approximately 17-19 °C/s at intermediate and late times. Data shown in Figure 3 are for a low wind test (wind speed about 1 m/s). Data from a higher wind test (i.e., 6 m/s) showed similar results.

**Table 23: Energy Balance Method/Thin Plate Gage Uncertainty –
Low Wind Case, Early Times**

Parameter	Value	Comments
ϵ	0.85	Pyromark paint emissivity
$\Delta\epsilon$	± 0.09	10% uncertainty from measurements (ref. [19])
h	0.021 kW/m ² -K	Maximum value from Table 5.
Δh	± 0.010 kW/m ² -K	50% uncertainty
T_s	300 K	Surface temperature at ambient
ΔT_s	± 15 K	Assume 5% uncertainty
T_∞	1300 K	Free stream gas temperature
ΔT_∞	± 325 K	Assumed variation in gas temperature, $\pm 25\%$
ρc_p	3760 kJ/m ³ -K	From ref. [5]
$\Delta \rho c_p$	± 188 kJ/m ³ -K	Assume 5% uncertainty
L	0.000254 m	Plate thickness 0.010" from [5]
ΔL	± 0.0000254 m	Assume 10% uncertainty from ref. [3]
k_{ins}	2.4E-05 kW/m-K	From ref. [5]
Δk_{ins}	$\pm 4.8E-06$ kW/m-K	Assume 20% uncertainty from ref. [5]
$T_{s,t} = \partial T_s / \partial t$	40 K/s	Approximate value inferred from ref. [5], Figure 12, and from Blanchat ⁹ (Figure 3)
$\Delta T_{s,t}$	± 22 K/s	Large uncertainty from experimental data (Figure 3)
$T_{ins,z} = \partial T_{ins} / \partial z$	200,000 K/m	Estimated from ref. [5], Figure 13
$\Delta T_{ins,z}$	$\pm 100,000$ K/m	Large uncertainty assumed, $\pm 50\%$

⁹ Unpublished experimental data from Dr. T. Blanchat, February 2005.

**Table 24: Relative Importance of Uncertainty Terms,
Energy Balance Method/Thin Plate Gage, Low Wind, Early Times**

Term	% of Total
$(\partial q_{inc,r} / \partial h) \Delta h)^2 / \Delta q_{inc,r}^2$	16.2
$(\partial q_{inc,r} / \partial \varepsilon) \Delta \varepsilon)^2 / \Delta q_{inc,r}^2$	0.9
$(\partial q_{inc,r} / \partial T_s) \Delta T_s)^2 / \Delta q_{inc,r}^2$	0.0
$(\partial q_{inc,r} / \partial \rho c_p) \Delta \rho c_p)^2 / \Delta q_{inc,r}^2$	0.6
$(\partial q_{inc,r} / \partial L) \Delta L)^2 / \Delta q_{inc,r}^2$	2.4
$(\partial q_{inc,r} / \partial k_{ins}) \Delta k_{ins})^2 / \Delta q_{inc,r}^2$	0.1
$(\partial q_{inc,r} / \partial T_\infty) \Delta T_\infty)^2 / \Delta q_{inc,r}^2$	7.5
$(\partial q_{inc,r} / \partial T_{s,t}) \Delta T_{s,t})^2 / \Delta q_{inc,r}^2$	71.4
$(\partial q_{inc,r} / \partial T_{ins,z}) \Delta T_{ins,z})^2 / \Delta q_{inc,r}^2$	0.9
All	100.0

Pool HFGs, Surface Temperature Time Derivative, Low Wind Test #1

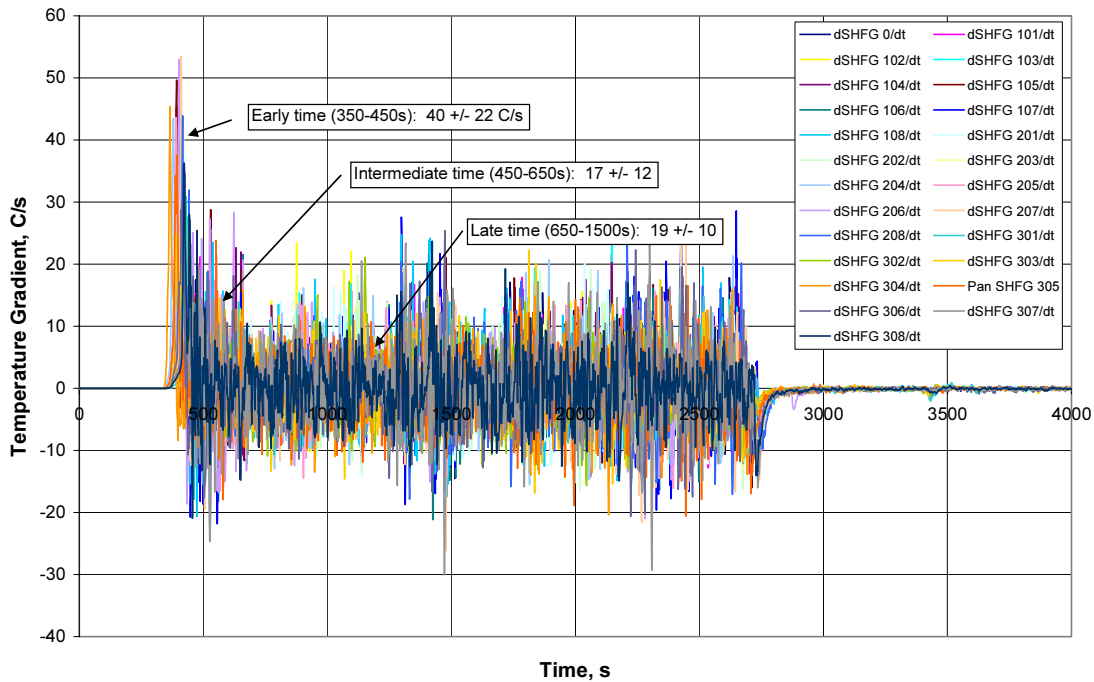


Figure 3: Estimate of Surface Temperature Temporal Gradient for Thin Plate Gage, Low Wind Fire

7.3.1.2 Intermediate Times

Table 25 shows the inputs for intermediate times, and Table 26 the relative importance of each uncertainty source.

**Table 25: Energy Balance Method/Thin Plate Gage Uncertainty –
Low Wind Case, Intermediate Times**

Parameter	Value	Comments
ϵ	0.85	Pyromark paint emissivity
$\Delta\epsilon$	± 0.09	10% uncertainty from measurements (ref. [19])
h	0.021 kW/m ² -K	Maximum value from Table 5.
Δh	± 0.010 kW/m ² -K	50% uncertainty
T_s	800 K	Surface temperature at ambient
ΔT_s	± 40 K	Assume 5% uncertainty
T_∞	1300 K	Free stream gas temperature
ΔT_∞	± 325 K	Assumed variation in gas temperature, $\pm 25\%$
ρc_p	4604 kJ/m ³ -K	From experimentally measured data
$\Delta \rho c_p$	± 230 kJ/m ³ -K	Assume 5% uncertainty
L	0.000254 m	Plate thickness 0.010"
ΔL	± 0.0000254 m	Assume 10% uncertainty from ref. [3]
k_{ins}	1.16E-04 kW/m-K	From ref. [5]
Δk_{ins}	$\pm 2.32E-05$ kW/m-K	Assume 20% uncertainty from ref. [5]
$T_{s,t} = \partial T_s / \partial t$	17 K/s	Approximate value inferred from ref. [5], Figure 12, and from Blanchat ⁹ (Figure 3)
$\Delta T_{s,t}$	± 12 K/s	Large uncertainty from experimental data (Figure 3)
$T_{ins,z} = \partial T_{ins} / \partial z$	100,000 K/m	Estimated from ref. [5], Figure 13
$\Delta T_{ins,z}$	$\pm 50,000$ K/m	Large uncertainty assumed, $\pm 50\%$

**Table 26: Relative Importance of Uncertainty Terms,
Energy Balance Method/Thin Plate Gage, Low Wind, Intermediate Times**

Term	% of Total
$(\partial q_{inc,r} / \partial h) \Delta h)^2 / \Delta q_{inc,r}^2$	7.3
$(\partial q_{inc,r} / \partial \varepsilon) \Delta \varepsilon)^2 / \Delta q_{inc,r}^2$	1.4
$(\partial q_{inc,r} / \partial T_s) \Delta T_s)^2 / \Delta q_{inc,r}^2$	6.7
$(\partial q_{inc,r} / \partial \rho c_p) \Delta \rho c_p)^2 / \Delta q_{inc,r}^2$	0.3
$(\partial q_{inc,r} / \partial L) \Delta L)^2 / \Delta q_{inc,r}^2$	1.2
$(\partial q_{inc,r} / \partial k_{ins}) \Delta k_{ins})^2 / \Delta q_{inc,r}^2$	1.6
$(\partial q_{inc,r} / \partial T_\infty) \Delta T_\infty)^2 / \Delta q_{inc,r}^2$	13.7
$(\partial q_{inc,r} / \partial T_{s,t}) \Delta T_{s,t})^2 / \Delta q_{inc,r}^2$	57.9
$(\partial q_{inc,r} / \partial T_{ins,z}) \Delta T_{ins,z})^2 / \Delta q_{inc,r}^2$	9.9
All	100.0

For the intermediate time, the total uncertainty is about ± 21.7 kW/m², or about 24% of the total. Table 26 shows again the importance of accurately measuring the temporal gradient of the plate temperature. Next in importance is the free stream gas temperature, then the insulation temperature gradient, and last the convective heat transfer coefficient.

7.3.1.3 Late Times

Table 27 shows the parameter values for late times, and Table 28 the relative importance of each uncertainty source.

**Table 27 Energy Balance Method/Thin Plate Gage Uncertainty –
Low Wind Case, Late Times**

Parameter	Value	Comments
ε	0.85	Pyromark paint emissivity
$\Delta \varepsilon$	± 0.09	10% uncertainty from measurements (ref. [19])
h	0.021 kW/m ² -K	Maximum value from Table 5.
Δh	± 0.010 kW/m ² -K	50% uncertainty
T_s	1300 K	Surface temperature at ambient
ΔT_s	± 65 K	Assume 5% uncertainty
T_∞	1300 K	Free stream gas temperature
ΔT_∞	± 325 K	Assumed variation in gas temperature, $\pm 25\%$

Parameter	Value	Comments
ρc_p	5170 kJ/m ³ -K	From experimentally measured data
$\Delta\rho c_p$	±260 kJ/m ³ -K	Assume 5% uncertainty
L	0.000254 m	Plate thickness 0.010"
ΔL	±0.0000254 m	Assume 10% uncertainty from ref. [3]
k_{ins}	2.6E-04 kW/m-K	From ref. [5]
Δk_{ins}	±5.2E-05 kW/m-K	Assume 20% uncertainty from ref. [5]
$T_{s,t} = \partial T_s / \partial t$	19 K/s	Approximate value inferred from ref. [5], Figure 12, and from Blanchat ⁹ (Figure 3)
$\Delta T_{s,t}$	±10 K/s	Large uncertainty from experimental data (Figure 3)
$T_{ins,z} = \partial T_{ins} / \partial z$	26,670 K/m	Estimated from ref. [5], Figure 13.
$\Delta T_{ins,z}$	±1,335 K/m	Large uncertainty assumed, ±50%

**Table 28 Relative Importance of Uncertainty Terms,
Energy Balance Method/Thin Plate Gage, Low Wind, Late Times**

Term	% of Total
$(\partial q_{inc,r} / \partial h) \Delta h)^2 / \Delta q_{inc,r}^2$	0.0
$(\partial q_{inc,r} / \partial \varepsilon) \Delta \varepsilon)^2 / \Delta q_{inc,r}^2$	1.0
$(\partial q_{inc,r} / \partial T_s) \Delta T_s)^2 / \Delta q_{inc,r}^2$	76.8
$(\partial q_{inc,r} / \partial \rho c_p) \Delta \rho c_p)^2 / \Delta q_{inc,r}^2$	0.1
$(\partial q_{inc,r} / \partial L) \Delta L)^2 / \Delta q_{inc,r}^2$	0.6
$(\partial q_{inc,r} / \partial k_{ins}) \Delta k_{ins})^2 / \Delta q_{inc,r}^2$	0.2
$(\partial q_{inc,r} / \partial T_\infty) \Delta T_\infty)^2 / \Delta q_{inc,r}^2$	4.3
$(\partial q_{inc,r} / \partial T_{s,t}) \Delta T_{s,t})^2 / \Delta q_{inc,r}^2$	15.9
$(\partial q_{inc,r} / \partial T_{ins,z}) \Delta T_{ins,z})^2 / \Delta q_{inc,r}^2$	1.1
All	100.0

The total uncertainty is estimated to be 38.8 kW/m², or about 42% of the total radiative incident flux. At late times the dominant uncertainty source is the plate surface temperature, followed by the temporal plate surface temperature gradient. Other sources are small.

7.3.2 High Wind Fire

7.3.2.1 Early Times

Table 29 provides estimates for the parameters at early times in a high wind fire.

**Table 29 Energy Balance Method/Thin Plate Gage Uncertainty –
High Wind Case, Early Times**

Parameter	Value	Comments
ϵ	0.85	Pyromark paint emissivity
$\Delta\epsilon$	± 0.09	10% uncertainty from measurements (ref. [19])
h	0.031 kW/m ² -K	Maximum value from Table 5.
Δh	± 0.015 kW/m ² -K	50% uncertainty
T_s	300 K	Surface temperature at ambient
ΔT_s	± 15 K	Assume 5% uncertainty
T_∞	1300 K	Free stream gas temperature
ΔT_∞	± 325 K	Assumed variation in gas temperature, $\pm 25\%$
ρc_p	3760 kJ/m ³ -K	From experimentally measured data
$\Delta \rho c_p$	± 188 kJ/m ³ -K	Assume 5% uncertainty
L	0.000254 m	Plate thickness 0.010"
ΔL	± 0.0000254 m	Assume 10% uncertainty from ref. [3]
k_{ins}	2.4E-05 kW/m-K	From ref. [5]
Δk_{ins}	$\pm 4.8E-06$ kW/m-K	Assume 20% uncertainty from ref. [5]
$T_{s,t} = \partial T_s / \partial t$	176 °C/s	Approximate value inferred from ref. [5], Figure 12, and from Blanchat ⁹ (Figure 3)
$\Delta T_{s,t}$	± 97 °C/s	Large uncertainty from experimental data (Figure 3)
$T_{ins,z} = \partial T_{ins} / \partial z$	880,000 K/m	Estimated from ref. [5], Figure 13
$\Delta T_{ins,z}$	$\pm 440,000$ K/m	Large uncertainty assumed, $\pm 50\%$

In Table 29, the temporal gradient of the plate temperature was estimated by multiplying the gradient for low winds, early times (40°C/s) by the increase in overall flux level (443/100 = 4.43). Data from Blanchat for high wind fires⁹ resulted in very similar values for the temperature gradient

as shown previously for low wind fires. This is believed to be due to the gages being located at the pool level, and not affected by the wind. Therefore the higher, calculated values will be used.

At early times the surface temperature is low so emitted energy is small. Most of the energy heats the plate, so assuming the plate is a lumped mass the higher flux increases the temporal gradient. The uncertainty in the temporal gradient ($\pm 97^\circ\text{C/s}$) was estimated using the same ratio (4.43).

The total uncertainty for the high wind, early time case is about 117.1 kW/m^2 , or about $\pm 29\%$ of the total incident radiative value. Table 30 shows the relative contributions of each of the terms. The temporal gradient of the surface temperature was the most important uncertainty source, comprising 85% of the total. All other sources were each less than 10%.

Similarly, the spatial gradient in the insulation was increased by the same ratio (4.43). Even with these large values the relative importance of the insulation gradient (Table 30) is only 1.1%, so no further effort was expended to obtain better estimates of the insulation gradient.

**Table 30 Relative Importance of Uncertainty Terms,
Energy Balance Method/Thin Plate Gage, High Wind, Early Times**

Term	% of Total
$(\partial q_{inc,r} / \partial h) \Delta h)^2 / \Delta q_{inc,r}^2$	4.4
$(\partial q_{inc,r} / \partial \varepsilon) \Delta \varepsilon)^2 / \Delta q_{inc,r}^2$	3.0
$(\partial q_{inc,r} / \partial T_s) \Delta T_s)^2 / \Delta q_{inc,r}^2$	0.0
$(\partial q_{inc,r} / \partial \rho c_p) \Delta \rho c_p)^2 / \Delta q_{inc,r}^2$	0.9
$(\partial q_{inc,r} / \partial L) \Delta L)^2 / \Delta q_{inc,r}^2$	3.4
$(\partial q_{inc,r} / \partial k_{ins}) \Delta k_{ins})^2 / \Delta q_{inc,r}^2$	0.2
$(\partial q_{inc,r} / \partial T_\infty) \Delta T_\infty)^2 / \Delta q_{inc,r}^2$	1.7
$(\partial q_{inc,r} / \partial T_{s,t}) \Delta T_{s,t})^2 / \Delta q_{inc,r}^2$	85.4
$(\partial q_{inc,r} / \partial T_{ins,z}) \Delta T_{ins,z})^2 / \Delta q_{inc,r}^2$	1.1
All	100.0

7.3.2.2 Intermediate Times

Table 31 shows the inputs for intermediate times, and Table 32 the relative importance of each uncertainty source. The same ratio was again used to estimate the insulation spatial gradient and the temporal surface temperature gradient, although the rationale is not as strong as for early times.

For the intermediate time, the total uncertainty is about $\pm 85.0 \text{ kW/m}^2$, or about 21% of the total. Table 32 shows again the importance of knowing the temporal gradient of the plate temperature,

and in this case, the spatial gradient of the insulation temperature. All other sources contribute small amounts to the total uncertainty.

**Table 31 Energy Balance Method/Thin Plate Gage Uncertainty –
High Wind Case, Intermediate Times**

Parameter	Value	Comments
ε	0.85	Pyromark paint emissivity
$\Delta\varepsilon$	± 0.09	10% uncertainty from measurements (ref. [19])
h	0.031 kW/m ² -K	Maximum value from Table 5.
Δh	± 0.015 kW/m ² -K	50% uncertainty
T_s	800 K	Surface temperature at ambient
ΔT_s	± 40 K	Assume 5% uncertainty
T_∞	1700 K	Free stream gas temperature
ΔT_∞	± 425 K	Assumed variation in gas temperature, $\pm 25\%$
ρc_p	4604 kJ/m ³ -K	From experimentally measured data
$\Delta \rho c_p$	± 230 kJ/m ³ -K	Assume 5% uncertainty
L	0.000254 m	Plate thickness 0.010"
ΔL	± 0.0000254 m	Assume 10% uncertainty from ref. [3]
k_{ins}	1.16E-04 kW/m-K	From ref. [5]
Δk_{ins}	$\pm 2.32E-05$ kW/m-K	Assume 20% uncertainty from ref. [5]
$T_{s,t} = \partial T_s / \partial t$	75 K/s	Approximate value inferred from ref. [5], Figure 12, and from Blanchat ⁹ (Figure 3)
$\Delta T_{s,t}$	± 53 K/s	Large uncertainty from experimental data (Figure 3)
$T_{ins,z} = \partial T_{ins} / \partial z$	440,000 K/m	Estimated from ref. [5], Figure 13
$\Delta T_{ins,z}$	$\pm 220,000$ K/m	Large uncertainty assumed, $\pm 50\%$

7.3.2.3 Late Times

Table 33 shows the parameter values for late times, and Table 34 the relative importance of each uncertainty source. The total uncertainty is estimated to be 123.8 kW/m², or about 31% of the total radiative incident flux. At late times the dominant uncertainty source is the plate surface temperature, and then the temporal gradient of the plate temperature. The contribution from the temporal gradient of the plate temperature may be overstated in Table 34, because the value from

Table 33 is highly uncertain. However, the conclusion does not change, the temporal gradient of the plate temperature is a large contributor to the total uncertainty.

**Table 32 Relative Importance of Uncertainty Terms,
Energy Balance Method/Thin Plate Gage, Low Wind, Intermediate Times**

Term	% of Total
$(\partial q_{inc,r} / \partial h) \Delta h)^2 / \Delta q_{inc,r}^2$	3.5
$(\partial q_{inc,r} / \partial \varepsilon) \Delta \varepsilon)^2 / \Delta q_{inc,r}^2$	2.6
$(\partial q_{inc,r} / \partial T_s) \Delta T_s)^2 / \Delta q_{inc,r}^2$	0.5
$(\partial q_{inc,r} / \partial \rho c_p) \Delta \rho c_p)^2 / \Delta q_{inc,r}^2$	0.4
$(\partial q_{inc,r} / \partial L) \Delta L)^2 / \Delta q_{inc,r}^2$	1.5
$(\partial q_{inc,r} / \partial k_{ins}) \Delta k_{ins})^2 / \Delta q_{inc,r}^2$	2.0
$(\partial q_{inc,r} / \partial T_\infty) \Delta T_\infty)^2 / \Delta q_{inc,r}^2$	3.3
$(\partial q_{inc,r} / \partial T_{s,t}) \Delta T_{s,t})^2 / \Delta q_{inc,r}^2$	73.7
$(\partial q_{inc,r} / \partial T_{ins,z}) \Delta T_{ins,z})^2 / \Delta q_{inc,r}^2$	12.5
All	100.0

**Table 33 Energy Balance Method/Thin Plate Gage Uncertainty –
Low Wind Case, Late Times**

Parameter	Value	Comments
ε	0.85	Pyromark paint emissivity
$\Delta \varepsilon$	± 0.09	10% uncertainty from measurements (ref. [19])
h	0.031 kW/m ² -K	Maximum value from Table 5.
Δh	± 0.015 kW/m ² -K	50% uncertainty
T_s	1700 K	Surface temperature at ambient
ΔT_s	± 85 K	Assume 5% uncertainty
T_∞	1700 K	Free stream gas temperature
ΔT_∞	± 425 K	Assumed variation in gas temperature, $\pm 25\%$
ρc_p	5170 kJ/m ³ -K	From experimentally measured data
$\Delta \rho c_p$	± 260 kJ/m ³ -K	Assume 5% uncertainty
L	0.000254 m	Plate thickness 0.010"
ΔL	± 0.0000254 m	Assume 10% uncertainty from

Parameter	Value	Comments
		ref. [3]
k_{ins}	2.6E-04 kW/m-K	From ref. [5]
Δk_{ins}	$\pm 5.2E-05$ kW/m-K	Assume 20% uncertainty from ref. [5]
$T_{s,t} = \partial T_s / \partial t$	84 K/s	Approximate value inferred from ref. [5], Figure 12, and from Blanchat ⁹ (Figure 3)
$\Delta T_{s,t}$	± 44 K/s	Large uncertainty from experimental data (Figure 3)
$T_{ins,z} = \partial T_{ins} / \partial z$	118,000 K/m	Estimated from ref. [5], Figure 13
$\Delta T_{ins,z}$	$\pm 59,000$ K/m	Large uncertainty assumed, $\pm 50\%$

Table 34: Relative Importance of Uncertainty Terms, Energy Balance Method/Thin Plate Gage, Low Wind, Late Times

Term	% of Total
$(\partial q_{inc,r} / \partial h) \Delta h)^2 / \Delta q_{inc,r}^2$	0.0
$(\partial q_{inc,r} / \partial \varepsilon) \Delta \varepsilon)^2 / \Delta q_{inc,r}^2$	2.0
$(\partial q_{inc,r} / \partial T_s) \Delta T_s)^2 / \Delta q_{inc,r}^2$	62.4
$(\partial q_{inc,r} / \partial \rho c_p) \Delta \rho c_p)^2 / \Delta q_{inc,r}^2$	0.3
$(\partial q_{inc,r} / \partial L) \Delta L)^2 / \Delta q_{inc,r}^2$	1.1
$(\partial q_{inc,r} / \partial k_{ins}) \Delta k_{ins})^2 / \Delta q_{inc,r}^2$	0.3
$(\partial q_{inc,r} / \partial T_\infty) \Delta T_\infty)^2 / \Delta q_{inc,r}^2$	1.6
$(\partial q_{inc,r} / \partial T_{s,t}) \Delta T_{s,t})^2 / \Delta q_{inc,r}^2$	30.2
$(\partial q_{inc,r} / \partial T_{ins,z}) \Delta T_{ins,z})^2 / \Delta q_{inc,r}^2$	2.1
All	100.0

8 Discussion

Table 35 provides a summary of the uncertainty estimates for all the types of measurement techniques, in both wind conditions, for all three times. Table 36 shows which parameters have the greatest effect on the total uncertainty.

Table 35 Summary of Uncertainty Estimates for Incident Radiative Flux

Time Period	S-B Type Gage	Calorimeter & Inverse Heat Conduction Method	Thin Plate/Energy Balance Method
Low Wind			
Early times	±39%	±34%	±32%
Intermediate Times	±39%	±27%	±24%
Late Times	±39%	±40%	±42%
High Wind			
Early times	±23%	±27%	±29%
Intermediate Times	±23%	±25%	±21%
Late Times	±23%	±25%	±31%

Table 36 Parameters Having Largest Effect on Total Uncertainty

Low and High Winds	Early Time	Intermediate Time	Late Time
S-B Gage	1) Net flux 2) Surface emissivity	1) Net flux 2) Surface emissivity	1) Net flux 2) Surface emissivity
Calorimeter & Inverse Heat Conduction Method	1) Net flux 2) Surface emissivity	1) Net flux 2) Surface emissivity	1) Surface temperature 2) Net flux
Sandia HFG (thin plate)	1) Temporal surface temperature gradient 2) Convective HTC	1) Temporal surface temperature gradient 2) Free stream temperature	1) Surface temperature 2) Temporal surface temperature gradient

The estimated uncertainties from Table 35 for the S-B gage range from a low of about ±23% to a high of about ±39%. The uncertainty of the S-B type gage is constant at each of the respective wind speeds but is highest (±39%) at the low wind speed because the convective fraction is higher. The uncertainty drops to ±23% for the high wind case. Uncertainty in net heat flux and surface emissivity contribute most to the total for incident radiative heat flux for the S-B gage.

Uncertainty estimates vary when using the calorimeter/inverse heat conduction method, from a low of ±25% to a high of ±40%. At early and intermediate times the uncertainty in net flux and emissivity are most important to the total. At late times the surface temperature measurement contributes most to the total uncertainty. The uncertainty for the calorimeter in either low or high winds is likely lower than shown in Table 35 because measurement techniques have improved. An extensive analysis of TC bias errors when using TCs on an inconel or stainless steel plate was made in ref. [19]. After correcting for these bias errors, one might be able to reduce the assumed

$\pm 5\%$ uncertainty of surface temperature measurements by half, to 2.5% . This would significantly reduce the uncertainties at late times when using a calorimeter.

For either the S-B gage or calorimeter, uncertainty in heat transfer coefficient 'h' and gas temperature T_∞ have only a small effect on the total uncertainty in incident radiative flux. This result is fortunate because those two parameters exhibit large variations in a fire, and obtaining more precise values would be difficult.

For the thin plate type gage, the uncertainty ranged from $\pm 21\%$ to $\pm 42\%$. These values are comparable with those from either of the other two methods. However, the most important uncertainty sources are the temporal gradient of the surface temperature and the surface temperature. It is therefore not surprising that the thin plate gage response in the transient portion is poor (ref. [5]). Because S-B or Gardon type gages respond much faster than the Sandia HFG (thin plate), their transient response is much more accurate. The inverse heat conduction calorimeter also suffers from slow transient response, and will not accurately predict fast varying heat flux. This slow response is mostly due to the slow TC response, as noted earlier.

All the values for heat flux uncertainty are higher than desired. There is no clear advantage of one method over the other for all cases. Each is superior to another depending on the application. In one respect, the S-B type gage is more desirable because the uncertainty does not change with time in the fire, and it has better transient response. In another respect, the calorimeter is more desirable because it does not require water cooling and does not suffer from different calibration constants for radiation and convection. In steady fires the Sandia HFG is superior, but it is large (i.e., 4"x4"x4") compared to the S-B type gages (e.g., 1" diameter x 2" long). Calorimeters are generally largest, but are easy to fabricate and are inexpensive to build.

Because fires in the open are very dependent on the wind, and large fluctuations are typical, gages that only work well in steady environments (e.g., Sandia HFGs) are likely not the best choice. However, in sooty environments, water-cooled gages are not suitable because the sensing surface becomes covered with soot, changing the calibration.

Because hydrocarbon fuel fire environments are so severe, and because a number of problems can occur, it is suggested that multiple methods be used whenever possible. If the S-B gage were to foul due to soot buildup, the gage output would steadily decline. In that case the calorimeter results could be used. If space were limited, the calorimeter would probably be too large, so the Sandia HFG would be more appropriate. If 2-dimensional effects are large, then the use of a 1-dimensional inverse heat conduction code would not be appropriate. If all three methods are used, and the results agree to within their respective uncertainty bounds, then one has higher confidence in the flux measurements.

These uncertainties, when compared on an equal basis (i.e., 95% coverage level), are consistent with the results of ref. [12].

9 Conclusions

- 1) The uncertainty in incident radiative flux, applicable to S-B gages and inverse heat conduction methods, has the following contributors (in approximate order of importance):
 - a. Uncertainty in net heat flux;
 - b. Uncertainty of surface emissivity;
 - c. Uncertainty of surface temperature;
 - d. Uncertainty of convective heat transfer coefficient; and
 - e. Uncertainty of free stream gas temperature

- 2) The uncertainty in incident radiative flux, applicable to the thin plate/energy balance method, has the following contributors (most in order of importance):
 - a. Uncertainty in temporal surface temperature gradient;
 - b. Uncertainty of surface emissivity;
 - c. Uncertainty of surface temperature;
 - d. Uncertainty of convective heat transfer coefficient;
 - e. Uncertainty of free stream gas temperature;
 - f. Uncertainty in spatial gradient of insulation temperature;
 - g. Uncertainty in plate thickness;
 - h. Uncertainty in density*specific heat product; and
 - i. Uncertainty in insulation thermal conductivity

- 3) Uncertainty for S-B type gages is about $\pm 39\%$ at all times in the fire, for low winds, and about $\pm 23\%$ at all times for high winds.
- 4) For all times and in low and high winds, the uncertainty in incident radiative flux when using the S-B gage is most affected by the net flux uncertainty and uncertainty in surface emissivity.
- 5) Uncertainty for calorimeter/inverse heat conduction method in low winds is about $\pm 34\%$ at early times, $\pm 27\%$ at intermediate times, and $\pm 40\%$ at late times in the fire. For high wind fires the values are $\pm 27\%$, $\pm 25\%$, and $\pm 25\%$ for the three times.
- 6) The uncertainty in incident radiative flux when using a calorimeter and an inverse heat conduction method is most affected by the net flux uncertainty and uncertainty in surface emissivity at early and intermediate times. At late times uncertainty in surface temperature is most important.
- 7) The uncertainty in the thin plate/energy balance method is $\pm 24\%$ to $\pm 42\%$ in low wind fires, and ± 21 to $\pm 31\%$ in high wind fires.
- 8) The uncertainty in incident radiative flux when using a thin plate gage and energy balance method is most affected by the temporal gradient of the surface temperature and the surface temperature. At early times the convective HTC is important, and at intermediate times the free stream temperature is also important.
- 9) The uncertainty in S-B gages is reduced to about $\pm 3-4\%$ if the radiative calibration sensitivity equals the convective sensitivity, or if the convective fraction is negligible.
- 10) Because the thin plate uncertainty is most affected by the temporal gradient of surface temperature, the thin plate gage suffers from poor transient response.

- 11) Phenomena not being addressed in the thin plate/energy balance model, for example the error caused by the TC mounted on the plate and the slow response of the relatively large TC, account for the majority of the error at early times.
- 12) To improve incident radiative heat flux estimates, resources should be focused on reducing uncertainties in the surface emissivity and net heat flux (S-B gage and calorimeter), and surface temperature and surface temperature gradient (thin plate gage).
- 13) Net heat flux uncertainties can be improved by more accurate temperature measurements.
- 14) Thin plate measurements can be improved by use of smaller TCs which will improve the thin plate temperature and temporal gradient measurements.
- 15) Uncertainties in convective HTC and free stream temperature are secondary contributors to the total uncertainty for S-B gages and calorimeters. They play a slightly larger role for the thin plate gage.
- 16) More effort should be expended to understand differences between radiative and convective gage calibration constants for S-B gages.
- 17) Multiple methods should be used wherever possible to increase confidence in the quality of the measurements.

10 References

- [1] J. V. Beck, "Users Manual for IHCP1D," a Program for Calculating Surface Heat Fluxes from Transient Temperatures Inside Solids, Beck Engineering Consultants Co., Okemos, Michigan, 48864, October 30, 1999.
- [2] B. F. Blackwell, R.W. Douglass, and H. Wolf, "A Users Manual for the Sandia One-Dimensional Direct and Inverse Thermal (SODDIT) Code," Sandia National Laboratories report SAND85-2478, UC-32, Printed May 1987, and Reprinted December 1980.
- [3] "Uncertainty Analysis of Heat Flux Measurements Estimated via a One-Dimensional, Inverse Heat-Conduction Program by V.G. Figueroa and J.T. Nakos, Fire Science and Technology, Department 9132, Sandia National Laboratories, and J.E. Murphy, Worcester Polytechnic Institute, SAND2005-0339, February 2005.
- [4] "Estimates of Error Introduced when One-Dimensional Inverse Heat Transfer Techniques are Applied to Multi-Dimensional Problems," by Carlos Lopez, Jorman Koski, and Arsalan Razani, Proceedings of NHTC'00, 34th National Heat Transfer Conference, Pittsburgh, PA, August 20-22, 2000.
- [5] "Sandia Heat Flux Gauge Thermal Response and Uncertainty Models", by T.K. Blanchat, L.L. Humphries, and W. Gill, Sandia National Laboratories report SAND2000-1111, May 2000.
- [6] "Heat flux measurement techniques," by P.R.N. Childs, J.R. Greenwood, and C.A. Long, Proceedings of the Institute of Mechanical Engineers, Volume 213, Part C, 1999.
- [7] Measurement Systems, Application and Design, Fourth Edition, by E.O. Doebelin, McGraw-Hill, 1990.
- [8] Informal communication, Dr. Tom Diller, Virginia Tech University, to Dr. Tom Blanchat, Sandia National Laboratories, May 2004.
- [9] "Analysis of Heat Flux Measurement by Circular Foil Gages in a Mixed Convection/Radiation Environment," by C.H. Kuo and A.K. Kulkarni, ASME/JSME Thermal Engineering Proceedings, Volume 5 – ASME 1991.
- [10] "A Convection Calibration Method for Local Heat Flux Gages," by G.J. Borell and T.E. Diller, ASME Journal of Heat Transfer, Transactions of the ASME, Vol. 109, February 1987, pp 83-89.
- [11] "Low Heat Flux Measurements: Some Precautions," A. F. Robertson and T. J. Ohlemiller, Fire Safety Journal 25 (1995), 109-124.
- [12] "Estimates of the Uncertainty of Radiative Heat Flux Calculated from Total Heat Flux Measurements," by R. Bryant, E. Johnsson, T. Ohlemiller, and C. Womeldorf, Building and Fire Research Laboratory, National Institute of Standards and Technology, Gaithersburg, MD, USA, reprinted from Interflam 2001, September 17-19, 2001, Edinburgh, Scotland.
- [13] ISO 9705, "Fire Tests – Full Scale Room Test for Surface Products," Geneva, Switzerland, 1993.
- [14] Experimental Methods for Engineers, Seventh Edition, by J.P. Holman, McGraw Hill, 2001.
- [15] "Test Uncertainty, Instruments and Apparatus," ASME PTC 19.1-1998.
- [16] Measurement Uncertainty, Methods and Applications, Second Edition, by Ronald H. Dieck, Instrument Society of America, 1997.

- [17] "Thermal Measurements in a Series of Large Pool Fires," by J.J. Gregory, R. Mata, and N.R. Keltner, SAND85-0196, August 1987.
- [18] Personal conversation with Dr. Alex Brown, Sandia National Laboratories, August 6, 2004. Estimates from VULCAN code predictions.
- [19] "Shroud Boundary Condition Characterization Experiments at the Radiant Heat Facility," by J.T. Nakos, J. Suo-Anttila, and W. Gill, Sandia National Laboratories report SAND2004-5080, October 2004.
- [20] Code of Federal Regulations, Energy, Part 10 CFR71.73, Nuclear Regulatory Commission, Revised January 1, 1999.
- [21] "Temporally Resolved Radiation Spectra from a Sooting, Turbulent Pool Fire," Proceedings of 2001 ASME International Engineering Congress and Exposition, November 11-16, New York, NY, 2001.
- [22] "Thermal Measurements for a JP-8 Pool Fire in Cross-Flow with a C-141 Fuselage Section Located on the Leeward Edge," Sandia National Laboratories report SAND2001-0313, by Jill Suo-Anttila and Lou Gritzko, February 2001.
- [23] "The Radiative-Convective Partitioning of Heat Transfer to Structures in Large Pool Fires," by J.T. Nakos and N.R. Keltner, ASME HTD, Vol. 106, Heat Transfer Phenomena in Radiation, Combustion, and Fires, R.K. Shah Editor, Book Number H00498, 1989.
- [24] Fundamentals of Heat and Mass Transfer, Fifth Edition, by F.P. Incropera and D.P. Dewitt, John Wiley & Sons, 2002.
- [25] "Measurements of Gas Velocities and Temperatures in a Large Open Pool Fire," by M.E. Schneider and L.A. Kent, Fire Technology, Vol. 25, No. 1, February 1989.
- [26] "Uncertainty Analysis of TC Measurements for Use in Normal and Abnormal Thermal Experiments at Sandia's Radiant Heat Facility and Lurance Canyon Burn Site, by J.N. Nakos, SAND2004-1023, April 2004.
- [27] "An Investigation of the Ability of a Thin Plate Heat Flux Device to Determine the Incident Heat Fluxes During Enclosure Fires," by P.F. Lennon and G.W.H. Silcock, International Journal on Engineering Performance-Based Fire Codes, Volume 3, Number 1, pp1-15, 2001.
- [28] H.W. Coleman, W. Glenn Steele, "Experimentation and Uncertainty Analysis for Engineers", 2nd ed., John Wiley & Sons Inc., New York, 1999.

J.F. Nagel	MS0481, 2137	Charles Hanks	MS1135, 1532
Tom Hendrickson	MS0481, 2137	Dann Jernigan	MS1135, 1532
Brad Boswell	MS0481, 2137	Sylvia Gomez	MS1135, 1532
Scott Slezak	MS0481, 2132	Richard Streit	MS1135, 1532
K. Hughes	MS9014, 8242	Robert Nichols	MS1135, 1532
Arthur Ortega	MS9014, 8242	Burl Donaldson	MS1135, 1532
Art Ratzel	MS0384, 1500	Kirk Jensen	MS1135, 1532
T.Y. Chu	MS0834, 1500	John Hewson	MS1135, 1532
Anthony Thornton	MS1135, 1530	Vern Nicolette	MS1135, 1532
Wahid Hermina	MS0834, 1510	David Sundberg	MS1135, 1532
Gene Hertel	MS0836, 1516	Victor Figueroa	MS1135, 1532
Lou Gritz	MS1135, 1532	Amalia Black	MS0828, 1533
Martin Pilch	MS0828, 1533	Vicente Romero	MS0828, 1533
Steve Heffelfinger	MS1135, 1534	James Nakos (5)	MS1135, 1532
Ken Erickson	MS0834, 1512		
Sean Kearney	MS0834, 1512	Tom Diller, Virginia Tech University	
Steve Trujillo	MS0834, 1512	Ned Keltner, Ktech Corp.	
Amanda Barra	MS0836, 1516	Ben Blackwell, Blackwell Engineering	
Barry Boughton	MS0836, 1516	Joe Hartman, NASA	
Dean Dobranich	MS0836, 1516	Fred Fisher, Fisher Research & Development, Inc.	
Ron Dykhuizen	MS0836, 1516	Larry Jones, Medtherm Corp.	
Bill Erikson	MS0836, 1516	Norman Alvares, Fire Science Applications	
Nick Francis	MS0836, 1516	Harry Hasagawa, FireQuest	
Roy Hogan	MS0836, 1516	John Hall, NFPA	
Walt Gill	MS0836, 1532	Marc Janssens, SwRI	
Cecily Glissman	MS0836, 1532	Rodney Bryant, NIST	
Tom Blanchat	MS1135, 1532		
Jill Suo-Anttila	MS1135, 1532		
Sheldon Tieszen	MS1135, 1532		
Alex Brown	MS1135, 1532		
Anay Luketa-Hanlin	MS1135, 1532		
		Central Technical Files, 8945-1 (2), MS9018	
		Technical Library, 4536 (2), MS0899	

